Anonymous 1

Submission on the proposal for "Blue Carbon Ecosystem Restoration Research Pilot Project" by Blue Carbon S2C Pty Ltd

The proposal

This project proposes hydrological modifications of coastal wetland landscapes to "restore" or create particular types of coastal wetlands on Kangaroo Island, Northern Territory as a pilot site for further project development in the NT (up to 39,000 ha). The aim of the project proponent is to use the *Tidal Restoration of Blue Carbon Ecosystems Methodology Determination 2022* (Emission Reduction Fund 2022) to obtain ACCUs, or international methods (e.g. VM0033 method under VERRA to gain VCUs), for coastal wetland restoration that are "restored" through hydrological modifications and other actions (e.g. planting).

Specifically the proposal aims to undertake:

1. Site identification of mangrove, saltmarsh, and supratidal forest habitats (i.e., blue carbon ecosystems) that are degraded or, at risk of further decline from either human or natural causes.
2. Restoration actions where specific restoration action or actions are carried out like hydrological rehabilitation that restores the hydrology by reconnecting water flows like de-silting natural canals and creating new canals.

The proponents have identified a pilot site with no evidence of human-altered hydrology (from freely available google earth images), and therefore I assume that the project proponents are planning to dredge (which is called de-silting) natural canals and/or create new canals, actions which will modify the hydrology of existing natural ecosystems, likely leading to the replacement of natural saltmarsh and sparsely vegetated saltmarshes (saltflats) with mangrove vegetation, as well as potentially pose risks to other connected floodplain ecosystems.

The proposed activities may not result in "restoration" or "rehabilitation" of existing vegetation (saltmarshes and saltflats) but likely to lead to afforestation by mangroves, which is the creation of mangrove forests over the existing natural ecosystem. Such afforestation may enhance carbon sequestration, but will have negative impacts on important saltmarsh and saltflat ecosystems and dependent ecological processes and communities, as well as enhancing the risk of saltwater intrusion on the landscape, which may threaten freshwater floodplain ecosystems.

Major comments

This proposal poses risks to natural saltmarsh and sparsely vegetated saltmarsh (saltflats) that have high ecological value (see Burford et al. 2016).

Conversion of one natural ecosystem into another for carbon credits is considered poor practice (e.g. see Blue Carbon standards https://www3.weforum.org/docs/WEF_HC_Blue_Carbon_2022.pdf and IUCN Nature Based Solution Standards https://portals.iucn.org/library/sites/library/files/documents/2020-020-En.pdf).

The High Quality Blue Carbon Principals and Guidance Standards recommend (page 15):

***Do no harm**. Project developers must avoid causing ecological disturbance or other environmental damage including, but not limited to, loss of biodiversity, habitat loss, habitat conversion, invasive or nonnative species introduction, reduced water quality, increased erosion, and increased net emissions.

The IUCN Nature Based Solutions Standards have the following criteria (page 10):

***Criterion 3: NbS result in a net gain to biodiversity and ecosystem integrity**

3.1 The NbS actions directly respond to evidence-based assessment of the current state of the ecosystem and prevailing drivers of degradation and loss.

Guidance: To develop a solution using nature, one must have a well-founded understanding of the current state of the ecosystems concerned. The baseline assessment needs to be broad enough to characterise ecological state, drivers for ecosystem loss and options for net improvements, making use of both local knowledge and scientific understanding where possible.

Detailed comments

- Given that human alteration of hydrology has not occurred at the pilot site and that there is no evidence of 39,000 ha of human altered coastal landscapes, see Groom et al. 2023 for a preliminary assessment of blue carbon opportunities in the NT, then we must assume that the proponents are planning to target sites with what they consider have "natural" hydrological restrictions, which include saltmarshes and sparsely vegetated areas (also called high intertidal saltflats).
- Saltmarshes and saltflats are sites that have natural restrictions to tidal flows that limit vegetation development, but they have high ecological value despite low vegetation cover (Burford et al. 2016, Lovelock et al. 2010), and are not degraded. They are important for regulation of floodwaters, for biogeochemical cycling and provide important habitat for many species when flooded.
- Parts of the proposed site is mapped as saltmarsh in the new Australian saltmarsh map. This map has not been officially released, but has been submitted to the Emission Reduction Fund. Although mapping of saltmarshes is difficult because of limited training data in northern Australia, the map suggests the proposed site is comprised of saltmarsh and saltflats.
- The concern for this proposed project is that the project proponents are targeting areas that saltmarshes and sparsely vegetated saltmarshes (or saltflats) which have low vegetation cover because they are naturally isolated from frequent tidal inundation, under the misguided idea that these are somehow degraded habitats, which they are not (Burford et al. 2016, Woodroffe et al. 2020). Hydrology will be altered by either dredging canals (called de-silting) or digging canals to increase tidal ingress, which will create areas that will be suitable for mangrove colonisation on what were natural saltmarshes and saltflats. This kind of activity may deliver high levels of ACCUs/VCUs (because mangroves sequester more carbon than saltmarshes or saltflats, Lovelock et al. 2022), but the activity of dredging canals and digging canals will essentially replace a natural ecosystem with another.
- By digging and dredging canals the project proponents will be speeding up the process of sea level rise on the landscape, facilitating seawater inundation of the landscape (Knighton et al. 1991, Saintilan et al. 2019). Digging and dredging canals will potentially result in increased tidal influence on connected freshwater floodplain ecosystems which are important for biodiversity and cultural heritage (Saintilan et al. 2019).
- Coastal ecosystems in the NT are strongly influenced by seasonal and interannual variation in sea level, rainfall and water flows (Abhik et al. 2021, Asbridge et al. 2019, Lymburner et al. 2019) and therefore exhibit high levels of seasonal and interannual variation in vegetation

cover. The widespread mangrove dieback in 2015-2016 was due to an extreme el Nino event with low sea levels and rainfall (Abhik et al. 2021, Chung et al. 2022). It was preceded by decades of earlier natural mangrove expansion (Asbridge et al. 2019). The project proponents propose to dredge and dig canals to reduce the impacts of extreme el Nino events. Canals are unlikely to influence the impacts of low sea levels on seaward fringing mangroves (where much of the mortality in 2015-2016 occurred), but are likely to enhance mangrove expansion within high intertidal saltmarsh and saltflat ecosystems, accelerating the impacts of sea level rise.

- The proponents use the Gulf of Mexico as an example of where digging canals has been used in ecological restoration, however the situation in the Gulf of Mexico is entirely different to that in the Northern Territory. In the Gulf of Mexico mangrove areas have been exposed to human hydrological modifications often associated with infrastructure developments that combined with climate extremes have led to widespread mangrove mortality and soil subsidence (Valderrama-Landeros et al. 2020). In this case, restoration projects are attempting to recover mangrove cover. In contrast, the coastal wetlands of the Northern Territory are in a largely natural state. Digging canals will not return the landscape to a repaired state but instead put an extensive and risky human footprint on what are currently relatively undisturbed wetlands.

Suggestions for clarifications

1. Clarify what the "natural" restriction to tidal flows are at the pilot project site. Describe the elevational range and tidal inundation characteristics of the natural ecosystems that are evident in the baseline (an baseline assessment) that encompasses climatic variation (El Nino – la Nina cycles) and how these will be maintained with the proposed project activities. Ecosystems like saltmarshes and saltflats occur because of limited tidal inundation, which is normal along gradients in tidal inundation over the very extensive, flat intertidal zone of the project site.
2. Clarify where 39,000 ha of tidal restricted wetlands occur, and provide evidence that these are not natural saltmarshes and sparsely vegetated saltmarshes (saltflats). Consult with experts on the characteristics of coastal wetlands of the region to evaluate the state of these wetlands and the normal range of their variation over years.
3. Provide evidence that dredging (called "de-silting" in the proposal) and excavation of canals poses no threats to existing saltmarsh and saltflats or connected freshwater floodplain vegetation and biodiversity. Evidence could be evaluated by experts on coastal wetlands of the region and the hydrology of coastal floodplains of the region.
4. Experts that have published extensively on the coastal wetlands on the NT that could be consulted include Prof Kerrylee Rogers, University of Wollongong, kerrylee@uow.edu.au; Prof Colin Woodroffe, University of Wollongong, colin.woodroffe@uow.edu.au; and Prof Max Finlayson, Charles Sturt University, mfinlayson@csu.edu.au

References

Abhik, S., Hope, P., Hendon, H.H., Hutley, L.B., Johnson, S., Drosdowsky, W., Brown, J.R. and Duke, N.C., 2021. Influence of the 2015–2016 El Niño on the record-breaking mangrove dieback along northern Australia coast. Scientific Reports, 11(1), p.20411.

Asbridge, E.F., Bartolo, R., Finlayson, C.M., Lucas, R.M., Rogers, K. and Woodroffe, C.D., 2019. Assessing the distribution and drivers of mangrove dieback in Kakadu National Park, northern Australia. Estuarine, Coastal and Shelf Science, 228, p.106353.

Burford, M.A., Valdez, D., Curwen, G., Faggotter, S.J., Ward, D.P. and Brien, K.O., 2016. Inundation of saline supratidal mudflats provides an important source of carbon and nutrients in an aquatic system. Marine Ecology Progress Series, 545, pp.21-33.

Chung, C.T., Hope, P., Hutley, L.B., Brown, J. and Duke, N.C., 2023. Future climate change will increase risk to mangrove health in Northern Australia. Communications Earth & Environment, 4(1), p.192.

Groom, R., Hutley, L.B., Brown, B., Lovelock, C. and Vickers, R., 2022. Blue Carbon in the Northern Territory, Australia: A review of the status and potential for blue carbon restoration. Charles Darwin University.

Knighton, A.D., Mills, K. and Woodroffe, C.D., 1991. Tidal-creek extension and saltwater intrusion in northern Australia. Geology, 19(8), pp.831-834.

Lovelock, C. E., Adame, M. F., Bradley, J., Dittmann, S., Hagger, V., Hickey, S. M., Hutley, L. B., Jones, A., Kelleway, J. J., Lavery, P. S., Macreadie, P. I., Maher, D. T., McGinley, S., McGlashan, A., Perry, S., Mosley, L., Rogers, K., & Sippo, J. Z. (2022). An Australian blue carbon method to estimate climate change mitigation benefits of coastal wetland restoration. Restoration Ecology, e13739. https://doi.org/10.1111/rec.13739

Lovelock, C.E., Grinham, A., Adame, M.F. and Penrose, H.M., 2010. Elemental composition and productivity of cyanobacterial mats in an arid zone estuary in north Western Australia. Wetlands Ecology and Management, 18, pp.37-47.

Lymburner, L., Bunting, P., Lucas, R., Scarth, P., Alam, I., Phillips, C., Ticehurst, C., & Held, A. (2020). Mapping the multi-decadal mangrove dynamics of the Australian coastline. Remote Sensing of Environment, 238, 111185. https://doi.org/10.1016/j.rse.2019.05.004

Saintilan, N., Rogers, K., Kelleway, J.J., Ens, E. and Sloane, D.R., 2019. Climate change impacts on the coastal wetlands of Australia. Wetlands, 39, pp.1145-1154.

Valderrama-Landeros, L.H., López-Portillo, J., Velázquez-Salazar, S., Alcántara-Maya, J.A., Troche-Souza, C., Rodríguez-Zúñiga, M.T., Vázquez-Balderas, B., Villeda-Chávez, E., Cruz-López, M.I. and Ressl, R., 2020. Regional distribution and change dynamics of mangroves in México between 1970/80 and 2015. Wetlands, 40, pp.1295-1305.

Woodroffe, C.D., Kumbier, K. and Rogers, K., 2020. Use of airborne Lidar to investigate mangrove accommodation space in macrotidal estuaries of northern Australia. Estuarine, Coastal and Shelf Science, 245, p.106988.

Vol. 545: 21–33, 2016
doi: 10.3354/meps11621

MARINE ECOLOGY PROGRESS SERIES
Mar Ecol Prog Ser

Published March 8

Inundation of saline supratidal mudflats provides an important source of carbon and nutrients in an aquatic system

M. A. Burford[1,*], D. Valdez[1], G. Curwen[1], S. J. Faggotter[1], D. P. Ward[1], K. R. O'Brien[2]

[1]Australian Rivers Institute, Griffith University, Kessels Rd, Nathan, QLD 4111, Australia
[2]School of Chemical Engineering, The University of Queensland, St Lucia, QLD 4075, Australia

ABSTRACT: Supratidal mudflats are a poorly understood habitat adjacent to coastal areas and are under pressure from human development and climate change. These habitats are only inundated infrequently but may be important contributors to coastal productivity. This study determined nutrient release and primary productivity (PP) on a large, pristine supratidal mudflat in the wet–dry tropics of Australia. Results of experimental studies on nutrient release and PP upon freshwater inundation were incorporated into a simple model of supratidal mudflat inundation based on remote sensing data and long-term river height data. The model was used to hind-cast potential annual primary production and nutrient release for a period capturing high and low inundation years. Our experimental studies measured a rapid release of nitrate, ammonium and phosphate in the first 2 d after inundation. Some days later there was measurable algal growth. Incorporating this data into the model showed that the main driver for the whole-system PP rates was the areal extent of inundation, rather than the duration of inundation, provided that inundation lasted longer than the minimum period for primary production to occur. The same was true for nutrient release although a shorter period of inundation was needed for release to occur. Future changes in flow and associated flooding, as a result of climate change and/or water resource development, could therefore have significant effects on productivity in these coastal systems.

KEY WORDS: Primary productivity · Benthic algae · Nitrogen · Phosphorus

INTRODUCTION

Coastal supratidal mudflats, otherwise known as supratidal mudflats or sabkhas (Briere 2000) are shallow coastal habitats only infrequently tidally inundated. However, during large rainfall events which result in overbank flow, or sustained local rainfall, they may be flooded for extended periods. There has been wide scale destruction and degradation of these habitats around the world due to human pressures on coastal areas (Halpern et al. 2008), including infilling for urban and agricultural development. Despite this, there is insufficient acknowledgement of their ecological value to coastal and estuarine ecosystems (Albuquerque et al. 2014).

Wet-dry tropical areas of Australia have extensive areas of supratidal mudflats which remain relatively pristine, and can therefore provide insights into the ecological value of this habitat. The few studies have shown that contributions of these habitats to coastal nutrient and carbon (C) biogeochemistry can be significant (Lovelock et al. 2010, Adame et al. 2012). The land adjacent to the Gulf of Carpentaria contains thousands of square kilometres of low-lying, supra-

*Corresponding author: m.burford@griffith.edu.au

tidal mudflats which are mostly vegetation free, and are coated in a salt crust for most of the year (Rhodes 1980). This habitat contains benthic algal species which remain dormant until there is rainfall and/or flooding, after which time algal growth occurs, although this has not previously been quantified. The nutrient biogeochemistry underpinning the algal growth is also poorly known with the exception of a study in the 1980s which found nutrient outwelling to adjacent coastal areas upon inundation (Ridd et al. 1988). It is likely that inundation of supratidal mudflats contributes to nutrient release fuelling primary production in the land–water interface of these coastal areas.

Our study therefore examined primary productivity (PP) and nutrient release from supratidal mudflats adjacent to an estuary in the Gulf of Carpentaria over 2 yr. We hypothesized that supratidal mudflats are a source of nutrients to adjacent coastal waters, and provide a food source directly or indirectly to higher trophic levels. Our approach was to combine experimental studies with river flow data and remote sensing estimates of inundation to determine potential annual areal PP and nutrient release, for the supratidal mudflats in an entire river-estuarine system.

MATERIALS AND METHODS

There were 4 main components to this study:

- PP, algal biomass and nutrient release were determined experimentally from wetted samples taken from supratidal mudflats across 3 consecutive years.
- Inundation area in the study catchment area was calculated from satellite imagery over 2 wet seasons, and correlated against river height measured at a river gauging station adjacent to the supratidal mudflats. This correlation was used to develop an inundation area model, which predicted the supratidal mudflat inundation area (SMIA) as a function of data on gauged river height, by subtracting the river channel area from the total inundation area.
- The inundation model was then applied to 36 yr of historical gauged river height data to hind cast annual SMIA and duration of inundation.
- Finally, the long-term inundation predictions were combined with the experimental measurements of PP, light attenuation and nutrient release to estimate long-term variability in PP and nutrient release associated with annual inundation patterns.

Study site

The study site was the tropical supratidal mudflats ('saline supratidal mudflats'; Rhodes 1980), adjacent to the Norman River estuary in the southern Gulf of Carpentaria, Australia (Fig. 1a). The Norman River estuary (17.463° S, 140.82° E) is a tropical tide-dominated estuary with mean rainfall of 913 mm (Normanton data, www.bom.gov.au) most of which falls during the summer monsoon period, but is highly

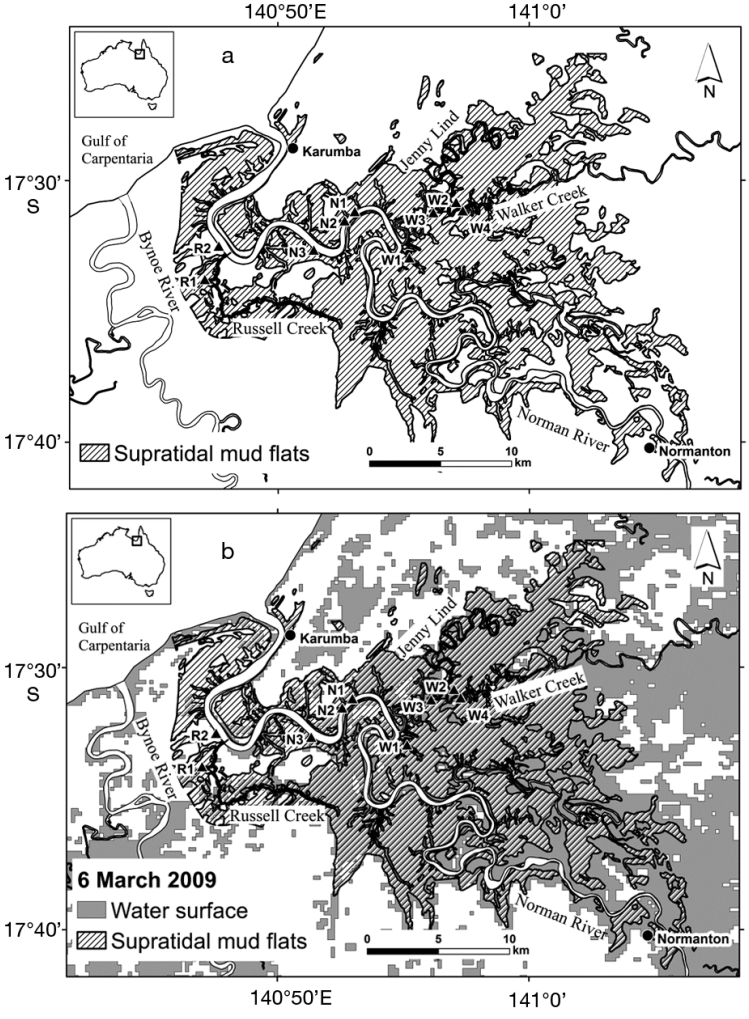

Fig. 1. Sampling sites on the supratidal mudflat adjacent to Walker Creek (W1–W4), Russell Creek (R1–R3) and Norman River (R1 and R2) on the Norman River estuary system, Gulf of Carpentaria, Australia. Supratidal mudflat in (a) the dry season, and (b) during a flood event in 2009

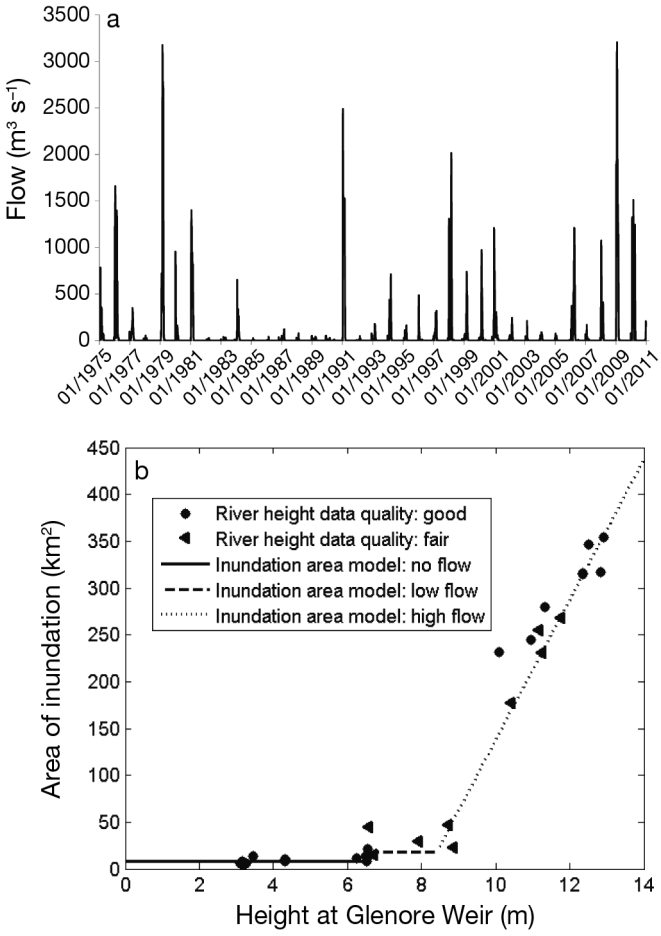

Fig. 2. (a) Hydrograph of river flow rates ($m^3 s^{-1}$) at Glenore Weir gauging station on the Norman River. (b) Relationship between water height (m) measured at Glenore weir and the inundation area (km^2) in the Norman River catchment estimated from remote sensing

intermittent from year to year (Fig. 2a) (Kennard et al. 2010). During our study, the wet season in Year 1 (2008–2009) had a major flood, while the second wet season (2009–2010) had a moderate flood (Fig. 1b; Duggan et al. 2014).

The estuary has a relatively simple morphology, with a main river channel (36 km^2), fringing tidal mudflats, a narrow strip of mangrove forest and beyond this, extensive supratidal mudflats (356 km^2) (National Land & Water Resources Audit 2001; http://trove.nla.gov.au/people/1306148?c=people). These supratidal mudflats are featureless with a slope as low as 3 cm km^{-1} (Rhodes 1980). In the dry season, the supratidal mudflats have a layer of dried salt. Tidal inundation only affects the supratidal mudflats at the highest astronomical tides, and forms the salt crust upon drying (Rhodes 1980). During annual wet seasons with sufficient rainfall, the supratidal mudflats are inundated as the high volumes of freshwater flowing downstream flood over the river channel and onto the mudflats, dissolving the salt (Burford et al. 2012). The low slope of the land means that large areas of supratidal mudflat (and terrestrial land) remain inundated with freshwater for days to months. The salt crust re-establishes in the dry season due to residual salt in the sediment, and further accumulates with subsequent high tides and evaporation.

Measurements of productivity and nutrient release

Sample collection

Surface soil samples were taken on supratidal mudflats adjacent to the Norman River system towards the end of the dry season in 3 consecutive years. In the first 2 yr (November 2008, November 2009), samples were taken for nutrient release and algal biomass experiments, and in the third year (June 2010) samples were taken for PP measurements. In the first 2 yr, 6 sites were sampled, 3 adjacent to the Norman River (N1, N2, N3), 2 adjacent to Russell Creek (R1, R2) and one in Walker Creek (W1) (Fig. 1). All sites had surface soil with similar characteristics, i.e. surface layer of dried salt with fine soil underneath. Two replicate samples of intact soil crust and associated biota were collected at each site, to a depth of 1–2 cm, over a total area of <5 m^2, and carefully placed in clear, shallow plastic trays ($20 \times 27 \times 3$ cm). The trays were stored in a cool dark place until experiments were conducted.

Nutrient release and algal growth experiments

Nutrient concentrations in the overlying water, and chlorophyll (chl) *a* concentrations in the soil samples, as a result of inundation of the tray samples, were determined. The trays were filled with distilled water to a depth of 2 cm. Trays were then incubated in direct sunlight. Distilled water was added each day to counteract evaporation. Distilled water was chosen to mimic the freshwater inundating the mudflats during the wet season (Burford et al. 2012). The tray water was subsampled (1 replicate from each of the 3 replicate trays) in Year 1 on Days 1, 2 and 7, and in Year 2 on Days 1, 2, 3, 5, 7 and 9, for dissolved inorganic nutrients (ammonium, nitrate/nitrite, phosphate) by filtering water through a 0.45 µm membrane filter, and freezing water samples at −20°C for subsequent analyses. Sediment chl *a* samples were

collected in Year 1 on Days 1, 3 and 7, and in Year 2 on Days 2, 4, 6 and 8. Sampling was done by pressing core tubes (2.4 cm dia.) randomly into the sediment, collecting the undisturbed top 1 cm of sediment. Samples were frozen at −20°C until analyzed.

At the end of each experiment, the salinity of the overlying water was determined using a calibrated probe (YSI). In the first experiment, salinity ranged from 44.3 to 107.7 (equivalent to ppt) while in the second experiment it ranged from 37.1 to 118.7. Temperature was also logged hourly (Thermochron iButton) and ranged from 26°C at night to a maximum of 46°C during the day.

Filtered nutrients were analyzed colorimetrically using standard laboratory methods and a flow injection analyzer (Greenburg et al. 2005). In the laboratory, chl *a* sediment samples were extracted in acetone using a probe sonicator (Branson 450) and measured spectrophotometrically (Shimadzu) at 665 and 750 nm, pre- and post- acidification to correct for phaeopigments (Jeffrey & Welshmeyer 1997).

Nutrient and chl *a* data from the supratidal mudflat experiments were tested for normality and square root transformed before conducting a Pearson's Correlation test (SAS software) to test for correlations between nutrients and chl *a*. Nutrient data from Day 2 was compared with chl *a* data on Day 3 (no data from Day 2) in the first year, and Day 8 (no data from Days 2 and 3) in the second year of experiments. Statistical analyses were also conducted, using an analysis of variance (R software; R Core Team 2015), to test for differences in both nutrient and chl *a* data between years, sites, and sampling occasions. Data was first tested for normality and log transformed.

To validate the experimental approach used to stimulate algal growth, sediment core samples were also taken for *in situ* chl *a* concentrations in soil samples at sites W1, W2, W3, W4 (Fig. 1) after an extended period of flooding in January 2009 and February 2010. Samples were analyzed for chl *a* using the same protocol as for the experimental samples. Secchi depth readings were done at the same time and used as input for the PP model.

Salinity experiment

The effect of salinity on benthic algal growth was determined by measuring changes in chl *a* concentrations in incubations of twenty cores (4.5 cm dia. Perspex cores) from one of the sampling sites (W1, Fig. 1). Salinity was measured after inundation of each core, with values ranging from 21.4 to 92.4. The same protocol was followed as outlined above for incubations of the tray samples.

Primary productivity experiments

In the third year (June 2010), tray experiments were conducted on soil samples collected from 2 sites, N1 and W4 (Fig. 1), to measure PP and respiration, as determined by oxygen fluxes under a range of light conditions over time. Experiments were conducted with 2 cm deep samples placed in clear 4.5 cm dia. Perspex cores, filled with deionized water and covered with clear plastic film to prevent evaporation losses. Cores were placed in a water bath set at a temperature of 30°C in direct sunlight. There were 5 light treatments: 100, 10, 1 and 0.5% sunlight and dark, with 4 replicates for each treatment. Neutral density filter sheets were used to create the appropriate light levels (Burford et al. 2012). Additionally, there were 2 controls, containing only deionized water and no soil. Oxygen production/consumption rates were quantified by measuring changes in the dissolved oxygen (DO) concentrations in the water overlying each core hourly over 5 h each morning for a total of 11 d under a diel cycle. DO was measured using a PreSens Microx TX3 and oxygen microsensor (PreSens Precision Sensing). Ambient light measurements were logged using the PAR light sensor (Licor LI-1400). Oxygen production and consumption rates, as mg O_2 l^{-1} h^{-1}, were calculated using a linear regression of DO vs. time. The volume was converted to the areal productivity and respiration based on the water volume, and surface area of the sediment in the core incubators. It was assumed that there was sufficient sunlight for PP for 10 h d^{-1}. Oxygen was converted to C based on a molar conversion ratio of 1:1. Analysis of variance testing was also conducted on log-transformed PP data using R software (R Core Team 2015) to test for differences between sites and light levels.

Inundation model development

An inundation model was constructed to predict SMIA as a function of daily river height measured at a gauging station situated at an overflow weir (Glenore Weir, 80 km from the mouth of the Norman River estuary; www.derm.qld.gov.au/water). The model was developed by quantifying the relationship between the water height at the river gauging station with total inundation area as calculated from satellite

images over the period October 2008 to 30 April 2010. The inundation model was then applied to predict annual inundation characteristics (including maximum area, depth and duration) based on gauging station data from 1975–2010. River channel area was subtracted from total inundation area to determine the SMIA.

Remote sensing to determine inundation area

Satellite imagery was used to estimate total inundation area within the Norman River catchment for 32 largely cloud-free images collected between 21 October 2008 and 30 April 2010, i.e. over the 2 wet seasons of the study. Area of land inundated by water was calculated from the MODIS Level 1B Calibrated Geolocation Data Set, which had pixel values converted to radiance. To maximize the resolution of the flood delineation, only MODIS 250 m resolution RED (band 1) and NIR (near infrared) (band 2) bands were used for image classification.

Spectral metrics, such as band ratios and difference indices using near infrared (NIR) spectral data (>800 nm), are commonly employed for delineating water features (McFeeters 1996, Frazier & Page 2000, Davranche et al. 2010). For this study, the Normalised Difference Vegetation Index (NDVI) and the NIR band were used to identify the extent of flood water. NDVI is calculated as NDVI = (NIR − RED)/ (NIR + RED) and is commonly applied as an indicator of live green vegetation (Defries & Townshend 1994). Free standing water has low reflectance in MODIS bands 1 and 2, and values of NDVI close to zero are indicative of water features and can be applied to delineate flood waters from surrounding land (Davranche et al. 2010, Ward et al. 2013).

Images were cropped to the broad region of interest (southern Gulf of Carpentaria). Histogram density slicing (Frazier & Page 2000) was applied to the NDIV and NIR data to delineate flood water. Density-slicing thresholds varied between images, and were manually checked against the coastline location to ensure that marine water was correctly delineated from terrestrial land. Images were then cropped to the Norman River catchment. Area of inundation was estimated as the area of pixels with NDVI less than the critical density slicing threshold. The same process was repeated using NIR for cross-validation. Local information (e.g. timing and duration of road closure due to flooding and discharge volume at Glenore Weir) was used to ground-truth the inundation area calculated from remote sensing. While all efforts were made to eliminate cloud cover, some images were processed with sparse cloud cover which was masked out and not included in image analysis.

The supratidal mudflat extent within the Norman catchment was defined using the Geoscience Australia 2006 GEODATA 250k topographic mapping (www.ga.gov.au/). The 'Saline Coastal Flat' feature class was used to delineate the supratidal mudflat extent with the addition of some 4% of the area comprising 'Swamp', and 'Land Subject to Inundation' classes that were either mislabeled or had changed since the original mapping in the late 1970s. The boundary of the supratidal mudflat extent was defined by the Norman river catchment boundary to the west. However, 2 tidal creeks occurred between the supratidal mudflat extent and the Norman river catchment boundary to the north east. Consequently, drainage lines and direction associated with the tidal creeks was used to define the north eastern boundary of the supratidal mudflat study area extent. The delineated total flood extent (including non-SMIA floodplains) for the Norman catchment was then 'clipped' to the supratidal mudflat study area extent for the inundation area model.

Correlating inundation area to gauged river height

Daily river height data is available for Glenore Weir (www.derm.qld.gov.au/water). The Department of Natural Resources and Mines designated the river height data quality in 3 categories: good; fair; poor; or estimate. Only good and fair data was used in the study (Fig. 2b).

The height of the Glenore weir was 6.4 m, meaning that when the water height was above 6.4 m, water was flowing over the weir. Between water heights of 6.5 and 8.4 m, flow was contained within the downstream river channel (www.derm.qld.gov.au/water). Above 8.4 m water height, the river was no longer contained in the channel. These river heights were therefore used to define 3 flow regimes at Glenore Weir: no (<6.5 m), low (6.5–8.4 m) and high flow (>8.4 m). Supratidal mudflat inundation was the area inundated, excluding the area of the river channel.

Estimated inundation area for 31 January 2012 was excluded from the analysis as an outlier, because despite the high flow through Glenore Weir (772–1030 $m^3 s^{-1}$ flow, 10.2–10.9 m height) over that day, the floodplain area of inundation was low. The source of this anomaly is not known, but it may relate to the timing of the satellite.

Long-term estimates of annual inundation

The inundation area model was applied to the river height gauge at Glenore Weir for the total period for which river height records are available, i.e. 1 July 1975 to 30 June 2012 (Fig. 2b). Data were integrated into an annual timestep based on water years, i.e. July to June, to capture the entire wet season in the austral summer (December to March) each year. The inundation area model was used to estimate the maximum area of floodplain inundated per year and was coupled with the data from experimental studies to determine nutrient release and PP.

For PP, the depth distribution of the inundated area and light attenuation with water depth *in situ* were both used. Secchi depth, as a measure of light attenuation through the water, was measured as 0.2–0.3 m on the inundated supratidal mudflats in January 2009 and February 2010. The average of these 2 Secchi depths was used to calculate the light attenuation coefficient (Chapra 1997).

RESULTS

Measurements of productivity and nutrient release

Ammonium, nitrate/nitrite and phosphate concentrations were measured in the overlying water after wetting the supratidal mudflat samples. Overall, ammonium concentrations were significantly higher in Year 1 than Year 2 ($p < 0.005$); conversely, nitrate/nitrite and phosphate concentrations were significantly higher in Year 2 than Year 1 ($p < 0.05$) (Fig. 3). In Year 1, ammonium, nitrate/nitrite and phosphate concentrations were highest on Day 2 ($p < 0.05$). In Year 2, there were more sampling days (Days 1, 2, 3, 5, 7, 9). Nitrate/nitrite leaching were highest early in the experiment; being statistically higher ($p < 0.05$) on Days 1, 2 and 3 compared with Day 9, while ammonium was statistically higher ($p < 0.05$) on Days 3 and 5 compared with all other days. Phosphate concentrations were highest later in the experiment, although there was no consistency in statistical differences between days. There

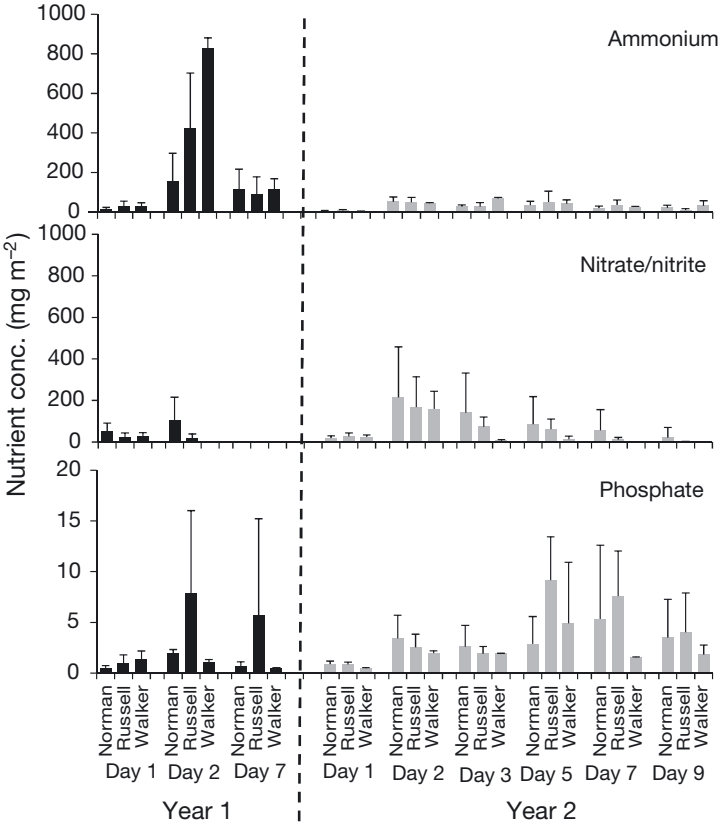

Fig. 3. Mean (+SD) ammonium, nitrate/nitrite and phosphate concentrations (mg m^{-2}) in water overlying sediments in tray experiments versus duration of inundation. Means were calculated from multiple trays in sites within supratidal mudflats adjacent to Russell (R1, R2) and Walker Creeks (W1), and the Norman River (N1, N2, N3; see Fig. 1 for site locations) for consecutive days in 2008/09 and 2009/10

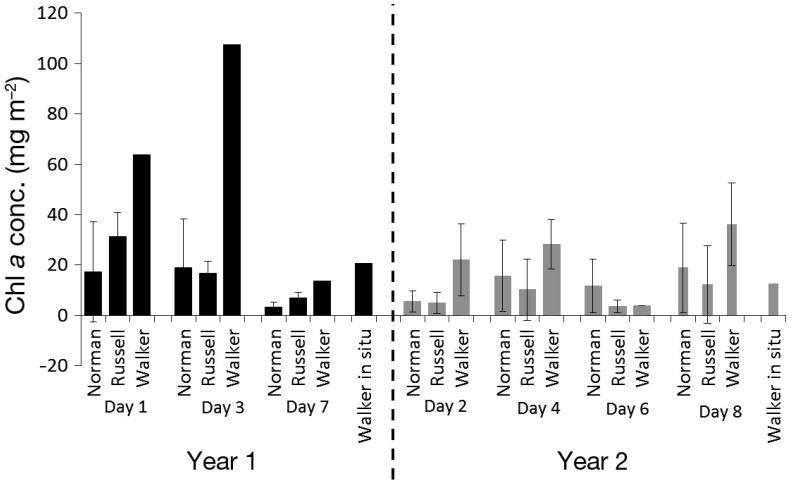

Fig. 4. Mean (±SD) chlorophyll (chl) *a* concentrations (mg m^{-2}) in sediments inundated for consecutive days in 2008/09 and 2009/10 during incubations. Samples were collected from supratidal mudflats adjacent to Russell and Walker Creeks, and the Norman River sites (see Fig. 1 for site locations). Additionally, *in situ* samples were collected from sites on Walker Creek during inundation for comparison with the experimental results

were no statistically significant differences between sampling sites within each year.

There were statistically significant differences in chl *a* concentrations between years ($p < 0.01$), but not between sites or sampling occasions (Fig. 4). The destructive sampling method means that even though sampling through time occurred within a small area (0.054 m^2), high spatial heterogeneity in the soil could not be avoided. Microscopic examination of samples revealed that the dominant benthic algal genera in the samples were the cyanobacteria *Oscillatoria* spp., *Geitlerinema* spp., and *Phormidium* spp. In a separate experiment using samples from one site, it was determined that there was no significant correlation between salinity (ranging from 21.4 to 92.4) in the water column and chl *a* concentrations in the sediment ($r^2 = 0.02$, $p > 0.05$).

Maximum chl *a* concentrations, i.e. Day 3 in Year 1, and Day 8 in Year 2, were compared with nutrient concentrations in the overlying water for the same days. Chl *a* was significantly and positively correlated with ammonium concentrations ($r^2 = 0.64$) but negatively correlated with nitrate/nitrite concentrations ($r^2 = -0.49$) (Table 1). There was no significant correlation between chl *a* and phosphate concentrations.

Table 1. Correlation between sediment chlorophyll (chl) *a* concentrations (measured on Day 3 in Year 1, Day 8 in Year 2), and nutrient concentrations (measured on Day 2 in both years) across multiple Norman River, Russell and Walker Creek sites (see Fig. 1) during supratidal mudflat inundation tray experiments (n = 12). $^{*}p < 0.05$, $^{***}p < 0.005$

Parameter	Ammonium	Nitrate/ nitrite	Phosphate
Chl *a*	**0.64*** **	**−0.49***	−0.32
Ammonium	–	**−0.45***	−0.12
Nitrate/nitrite	–	–	**0.41***

Table 2. Supratidal mudflat inundation area (SMIA) of the Norman River as a function of river height at Glenmore Weir (*h*, in metres) and associated flow regime

h (m)	Flow regime	Total inundation area (km^2)	SMIA (km^2)
<6.5	No flow over weir	8 ± 3 (river channel only)	0
6.5–8.4	Low flow	18 ± 6 (river channel only)	0
>8.5	High flow	$ah - b$ where $a = 75 \pm 10$ km^2 m^{-1}, $b = 613 \pm 114$ km^2 (river channel and flood plain)	$75 \times (h - 8.4)$

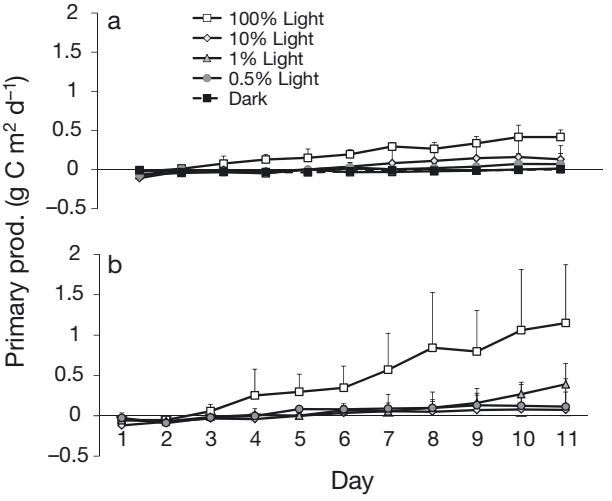

Fig. 5. Mean (+SD) primary productivity rates (g C m^{-2} d^{-1}) for supratidal sediments collected at (a) Site W4 near Walker Creek, and (b) Site N1 near the Norman River after continuous artificial inundation and exposure to a range of light levels on a diel cycle over 11 d

Ammonium and nitrate/nitrite concentrations were negatively correlated ($r^2 = -0.45$) while nitrate/nitrite and phosphate concentrations were positively correlated ($r^2 = 0.41$) (Table 1). In addition, chl *a* concentrations *in situ* during the wet season inundation in both years were found to be comparable with those in our experiment with artificial inundation (Fig. 4).

PP in the supratidal mudflat samples, as estimated from oxygen flux experiments, increased over the 11 d of the incubation study (Fig. 5). By Day 11, Site W4 had statistically higher productivity in 100% light than in 1 or 0.5% light ($p < 0.05$). In contrast, the high variability in replicate samples from Site N1 meant that there was no significant difference between light levels on Day 11 in samples. There was no significant difference between the 2 sites at 100% light on Day 11. Respiration reached a maximum by Day 1 for the dark treatments and ranged from 41.4 to 139.4 mg C m^{-2} d^{-1}.

Inundation model

The inundation area calculated from satellite imagery was strongly related to river height. For the high flow regime, the area inundated varied linearly with height of the river at Glenore Weir ($p < 0.001$) (Fig. 2b). The SMIA was therefore also a function of height at Glenore weir, and the equations are shown in Table 2.

Each additional 10 cm of river height at Glenore Weir when the river leaves the channel (i.e. at depths above 8.4 m) corresponds to a 7.5 km^2 increase in area of floodplain inundation. Hence if we assume a simple 'bathtub' model for bathymetry (which is not unreasonable given the very low vertical relief of the area), then the maximum depth of the floodplain (h_{max}) will be the difference between the river height at Glenore Weir, and the weir height (8.4 m).

Based on this model, a river height (h) of 9 m measured at Glenore Weir would correspond to an inundated area of SMIA = 45 km^2 and maximum water depth of h_{max} = 60 cm, with approximately 7.5 km^2 of increased inundation at each water depth increment of 10 cm.

Model results

Total nutrient loads for each year were calculated based on the model of inundation area of supratidal mudflats combined with the experimental data for minimum and maximum values for nutrient concentrations in the overlying water of mudflats on the day (Table 3). Nutrient concentrations were highly variable between years and on the sampling days but Day 2 was chosen as there was data from this day for both years. The annual nutrient release (t yr^{-1}) was hence calculated as:

$$ANR = ANF \times SMIA_{2d\ max} \quad (1)$$

where ANR is the annual nutrient release from the supratidal mudflats, ANF is the areal nutrient flux determined from the experimental studies, and $SMIA_{2d\ max}$ is the maximum SMIA which has been inundated for at least 2 consecutive days within the given year. Nutrient release rates where highly variable, so annual nutrient release was calculated from the data for both low and high nutrient release scenarios (Table 3).

Based on the model output, there is high interannual variability in the calculated mass of nutrients released from the supratidal mudflats, driven by the size of the flood event (Fig. 6). Maximum and minimum values ranged considerably for ammonium and nitrate/nitrite, based on the experimental results. Here was less variation for phosphate. Highest annual values of release were 166, 64 and 1.3 t for ammonium, nitrate/nitrite and phosphate respectively.

The experimental studies showed that benthic PP was affected by light levels (although only statistically significant for one of the 2 sites used in the experimental studies). However, modelling productivity based on light was not feasible, due to the uncertainty and variability in water clarity, and the inherent errors associated with such a simplistic model for depth distribution. Instead we used the average productivity (within the euphotic zone) recorded on Days 5 and 10 in the experimental studies, and assumed that this approximated the benthic productivity for inundated supratidal mudflats where at least 1% of light penetrated to the sediment (Table 3).

Five days was chosen as the minimum duration for initiating benthic productivity in the experiments. The effect of 10 d inundation was also chosen, based on the experimental data, to compare with 5 d and

Table 3. Parameters and rates used for nutrient and C model based on mean values on Day 2 for nutrients, and Days 5 and 10 for primary productivity (PP; mg C m^{-2} h^{-1}). ANF: areal nutrient flux (mg m^{-2}); CPI: critical period of inundation

Process	Scenario	Source	Inundation model
Ammonium ANF from sediment	Low: 48 High: 468	Tray incubations, multiple sites and replicates, 2 yr	• $SMIA_{2d\ max}$: maximum area of supratidal mudflats inundated for at least 2 consecutive days • Nutrients released no more than once per wet season
Nitrate/nitrite ANF from sediment	Low: 41 High: 180	Tray incubations, multiple sites and replicates, 2 yr	
Phosphate ANF from sediment	Low: 2.6 High: 3.6	Tray incubations, multiple sites and replicates, 2 yr	
Benthic PP	CPI = 5 d, PP_{5d} = 11 CPI = 10 d, PP_{10d} = 43	PP rates measured in core incubation experiments, at a range of light levels, on Days 5 and 10 of inundation	• $SMIA_{N\ euphotic}$: area of supratidal mudflats inundated for at least N = 5 or 10 consecutive days, integrated over the year CPI • Mean PP rates measured at 1 and 100% light for N = 5 or 10 d used for calculations

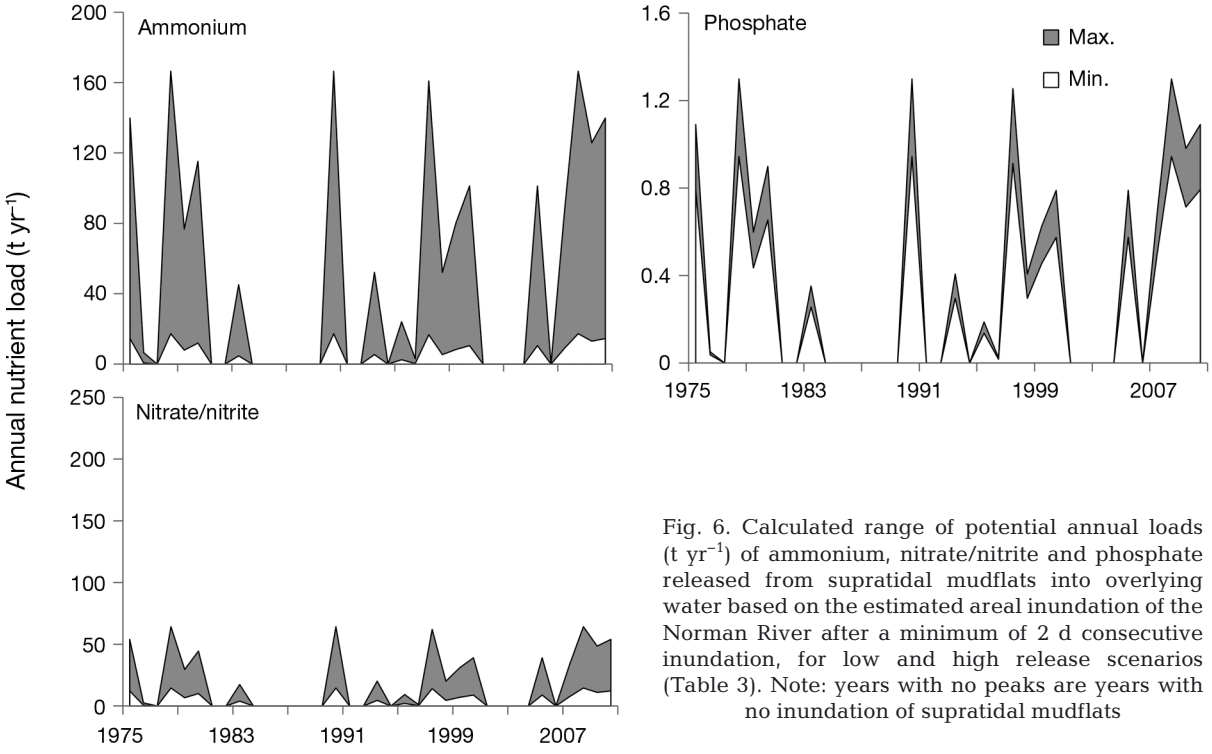

Fig. 6. Calculated range of potential annual loads (t yr^{-1}) of ammonium, nitrate/nitrite and phosphate released from supratidal mudflats into overlying water based on the estimated areal inundation of the Norman River after a minimum of 2 d consecutive inundation, for low and high release scenarios (Table 3). Note: years with no peaks are years with no inundation of supratidal mudflats

highlight the critical nature of inundation period in annual estimates. Therefore in estimating supratidal mudflat productivity, we ran the inundation model for two scenarios: productivity based on 5 and 10 d inundation respectively. The annual benthic productivity was calculated as follows:

$$ABP_N = PP_N \times SMIA_{N\ euphotic} \quad (2)$$

where ABP_N is annual benthic productivity, based on 5 or 10 d inundation, PP_N is areal primary productivity rate determined experimentally on Day N = 5 or 10, and $SMIA_{N\ euphotic}$ is the area of supratidal mudflats within the euphotic zone which has been inundated for more than 5 or 10 d respectively, integrated over the year. Soil is assumed to be dry if uncovered by water for >2 d.

Using Eq. (2), algal production was calculated for the whole Norman River supratidal mudflat system (356 km^2) using the mean of rates measured at 1 and 100% of surface light on Days 5 and 10 of the experiment, and a mean of 2 measured Secchi depths, 0.2 and 0.3 m *in situ*. Annual benthic algal production ranged between 0 t C in dry years up to 377 t C for the most productive years, provided there was a minimum of 5 d inundation (Fig. 7). For 10 d inundation period, maximum annual production was 273 t C. This value was lower than 5 d inundation because the probability of inundation for a longer period was lower.

DISCUSSION

This study showed that, after 48 h of inundation, there was substantial nutrient accumulation in overlying waters from seasonally inundated supratidal mudflats. However there was considerable variabil-

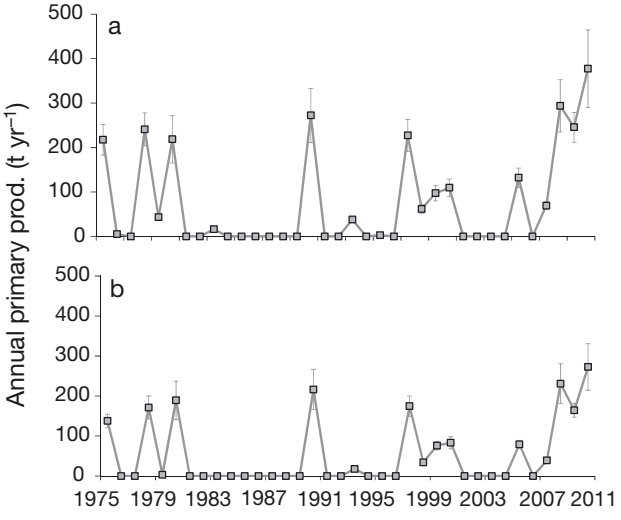

Fig. 7. Mean primary production (±SD) (t C yr^{-1}) based on the estimated areal inundation of the Norman River supratidal mudflat after (a) 5 d and (b) 10 d consecutive inundation. Mean value was calculated based on 2 scenarios of 0.2 and 0.3 m Secchi depth using the mean productivity at 1 and 100% light conditions in controlled experiments. Note: years with no peaks are years with no inundation of supratidal mudflats

ity between replicates, sites and years. This reflects the heterogeneity of the soil, and the observed fluctuations in topology as a result of sediment scouring and deposition during previous inundation events. The model output from our study also showed that there was a high level of interannual variability in released nutrients driven mostly by differences in inundation area between years. In a number of years, the lack of inundation resulted in no nutrient release.

The slow release of nutrients in our study contrasts with a study of tidally inundated cyanobacterial mats growing behind mangroves in a subtropical embayment, which had maximum release of phosphate, ammonium and nitrate after 1 h (Paling & McComb 1994). Additionally, the rates of release in their study were substantially lower (1 to 2 orders of magnitude) than in our study. However, these mats were inundated more frequently than those in our study, meaning that soil moisture and associated microbial activity at the time of inundation was initially likely to be higher, and nutrient reserves lower. Additionally, the standing stocks of cyanobacteria may also remain higher in their study since the mats do not become completely desiccated between inundation events.

Our study showed that PP on inundated supratidal mudflats in a wet–dry tropical system has the potential to be a significant contributor to primary production in coastal areas (up to an estimated 377 t C annual productivity in the Norman River supratidal mudflat system). However, primary production across the supratidal mudflats varied substantially from year to year, driven mostly by the scale of inundation during the wet season. In the study, there were multiple years with little or no inundation, e.g. 2001/02 to 2004/05, resulting in no calculated primary production. Therefore, the supratidal mudflats are highly dynamic systems both in the short and long term, with productivity driven in large part by the magnitude and duration of wet season flooding. Nutrient release from the mudflats is likely to be related to senescence and subsequent degradation of benthic algae from the previous season. As such, the scale of inundation from the previous year, and associated benthic algal growth, may affect nutrient release in the subsequent year.

The estimated annual PP rate and chl *a* concentrations of the supratidal mudflats were compared with results from previous studies in the same estuary for phytoplankton and benthic algae on intertidal mudflats (Table 4). Chl *a* concentrations on the intertidal mudflats were highest, i.e. 22.5–44.5 mg m^{-2}, followed by the supratidal mudflats (when inundated), i.e. 19.8 mg m^{-2}, then phytoplankton 9.2–19.2 mg m^{-2} (Burford et al. 2012, Duggan et al. 2014). PP per unit area was similar between the 3 habitats when supratidal mudflats in the wet season were compared with intertidal mudflats and phytoplankton in the dry season.

However, on an annual whole-system basis within the estuary, phytoplankton had the highest contribution to PP rates, i.e. 72–83%, compared to tidal mudflats, i.e. 15–17%. Supratidal mudflats ranged from 0% contribution in years with no inundation, to 13% of the total in years with inundation. However, while productivity on the supratidal mudflats only occurred in the wet season, most production in the intertidal mudflats and phytoplankton occurred in the dry season. Our figures are likely to be underestimates of the contribution of supratidal mudflats since our modelling was based on PP incubations which were only conducted for 11 d. Rates may have increased with longer periods of inundation, however, the frequency of longer term inundation per year would also decrease.

A study by Lovelock et al. (2010) measured PP rates of 26.6–95.6 mg C m^{-2} h^{-1} on tidal and supratidal flats in the arid subtropics of Western Australia, which were similar to our areal rates, i.e. 42.0–105.6 mg C m^{-2} h^{-1}. However, chl *a* concentrations were higher in their study than ours, i.e. 224–416 mg m^{-2} compared with 1.3–107.4 mg m^{-2}, respectively. A key difference between the studies was that the mudflats in

Table 4. Comparisons of chlorophyll (chl) *a* concentrations (mg m^{-2}), and areal and whole-system primary productivity (PP, mg C m^{-2} h^{-1} and tonnes C per season) in the supratidal mudflat and adjacent intertidal mudflats and estuarine water of the Norman River system. Whole-system PP refers to the combination of estuary, supratidal and intertidal mudflats. Wet: wet season; dry: dry season. Note: mangroves are not included as there is insufficient data

Habitat	Area (km^2)	Chl *a* (mg m^{-2})		Areal PP (mg C m^{-2} h^{-1})		Whole-system PP (t C per season)		Annual contribution to whole-system PP (%)	Reference
		Wet	Dry	Wet	Dry	Wet	Dry		
Supratidal mudflat	356	19.8	nd	43	0	0–377	0	0–13	This study
Intertidal mudflat	1	22.5	44.5	0	54	0	145	15–17	Duggan et al. (2014)
Phytoplankton	8	9.2	19.2	14	41	27	703	72–83	Burford et al. (2012)

their study were inundated more frequently than those in our study, meaning that the algal species in their study were likely to be more highly adapted to a rapid response to inundation. It took approximately 3 d for PP to commence in our study.

Paling et al. (1989) also found higher chl *a* concentrations of 50–150 mg m^{-2} for cyanobacterial mats in the Dampier Archipelago. They estimated that cyanobacterial mats contributed 5–15% of the total C fixed by primary producers in the entire coastal system. Lovelock et al. (2010) proposed that a significant proportion of the production by cyanobacteria on mudflats is allocated to extracellular carbohydrates which are released upon wetting. This in turn fuels the microbial community. It is likely that this mechanism is also occurring in our study, as microbial activity occurred very quickly after wetting of sediment, as indicated by the respiration rates of 41.4–139.4 mg C m^{-2} d^{-1} and net heterotrophic production in the first few days.

Our study found that a salinity ranging from 21 to 92 had no effect on chl *a* concentration. Therefore the benthic algal community appears to be highly adapted to high and variable salinities. Conversely, Kirkwood & Henley (2006) found a trend of declining chl *a* as salinity increased, although the salinity in their study was much higher, i.e. up to 350 in algal communities in a terrestrial hypersaline environment (Great Salt Plains, USA).

Ammonium had a strong positive correlation with chl *a* concentrations. One interpretation of this is that nitrogen is a limiting nutrient for benthic algae, and the ammonium is being rapidly assimilated. Ammonium is the form of nitrogen most easily assimilated by algae (Raven 1984, Dortch 1990), and can be released via desorption from soil, or from organic matter upon rewetting. Nitrate was negatively correlated with chl *a* concentrations, suggesting that nitrate was not the important source of nitrogen for benthic algal growth. Nitrate is often loosely bound to soil and released after rewetting. Understanding the sediment biogeochemistry as a result of wetting and drying and fluctuating salinity in these environments warrants more research.

The stoichiometric molar C:nitrogen ratio for algae (6.6:1; Redfield 1958) was also used to determine nitrogen requirements, calculated from measured areal rates of PP. This was compared with the total measured dissolved inorganic nitrogen released from the supratidal mudflats after wetting. Based on these calculations, dissolved inorganic nitrogen release from wetting only provides 2.9–6.6 d of nitrogen requirements for the benthic algae. This supports the argument for nitrogen limitation on the supratidal mudflats. Kirkwood & Henley (2006) also found that ammonium concentrations were an important predictor of algal biomass in a terrestrial hypersaline environment as did studies of cyanobacterial mats in the arid subtropics (Paling et al. 1989, Lovelock et al. 2010, Adame et al. 2012). The nitrogen:phosphorus ratios of the dissolved nutrients were much higher than Redfield (1958) ratios, which suggests that phosphorus, as well as nitrogen availability may also limit production, although the relatively high phosphate levels appear to discount this.

Nitrogen has been shown to be a key limiting nutrient in studies of the Norman River estuary, and the Gulf of Carpentaria as a whole (Burford et al. 2009, 2012). Total calculated nitrogen and phosphorus loads in freshwater discharged from the Norman River over the wet season were 4300 and 800 t respectively in 2008/09, and 2500 and 400 t respectively in 2009/2010 (Burford et al. 2012). Therefore river discharge provides an important nitrogen source to coastal areas in years where discharge occurs. Annual modelled nitrogen and phosphorus release across the supratidal mudflats in those years, assuming a minimum of 2 d of inundation, was approximately 1–8% and <1% of the total nitrogen and phosphorus discharge loads respectively for the river system across both years. Given the calculated nitrogen requirements of benthic algae on the supratidal mudflats, it cannot be assumed that all nitrogen is discharged into the river; mudflats may actually be a net sink for nitrogen. However, in a creek within the Norman River estuary, Ridd et al. (1988) found higher dissolved phosphate and nitrate/nitrite concentrations from water running off the supratidal mudflat on the ebb tide compared with the adjacent river. It is clear that further research on the sources, transformations and fate of nutrients in these supratidal mudflats and adjacent areas is needed.

Algal production on supratidal mudflats is likely to contribute to production by higher trophic levels in years where the inundation period is sufficiently long. A range of crustacean and fish species may access the supratidal mudflats during to feed during the period of inundation. Metapenaeid shrimp species were abundant in waters draining off these mudflats during the wet season (R. Kenyon pers. comm.). However, the links between PP and productivity in higher trophic levels is poorly understood and warrants further study in this system.

The processes that govern the benthic productivity on the Norman River supratidal mudflats are likely to be the same for other catchments in the southern

Gulf of Carpentaria. The extent of the supratidal mudflats in the southern Gulf of Carpentaria is contained largely within the Flinders-Norman, Mornington Inlet, and Nicholson-Leichhardt catchments. This is an area of 3458 km^2, based on the GEODATA 250k mapping of supratidal mudflat extents. Therefore PP across the southern Gulf could be as high as 748 t C in years where inundation is extensive and sustained, assuming uniformity in benthic algal biomass and responses to inundation.

Increasing development of coastal areas worldwide has dramatically reduced the area of coastal floodplains, including supratidal mudflats, as they have been traditionally considered as ecologically unimportant habitats. Additionally, water development, which reduces the scale of flooding, may also negatively impact the contribution of these habitats to coastal productivity (Fry 2002, Bayliss et al. 2014). Jardine et al. (2012) showed the critical importance of flooding of floodplains and connectivity to estuaries and coastal areas in supporting the growth and reproduction of a range of fish species, including commercially important species in the Gulf of Carpentaria.

In addition, future climate change impacts, such as changes in rainfall intensity, timing and duration, as well as sea level rise, are likely to have significant effects on supratidal mudflats. Projections for northern Australia include less frequent cyclones, which may reduce the scale of flooding (www.bom.gov.au/state-of-the-climate/). Conversely, greater and more sustained inundation will promote more production, while more variable climate regimes may reduce the frequency of rainfall, leading to less reliable productivity.

In summary, this study used a combination of experiments and modeling to provide estimates of PP and annual nutrient loads on supratidal mudflats in a wet–dry tropical river system. This study has highlighted that in years with sufficient inundation, these habitats may play an important role in coastal productivity.

Acknowledgements. We thank Melissa Duggan, Matthew Whittle, Robert Kenyon and Andy Revill for assistance with field work, Ken Tews for assistance with datalogger processing, Amanda Neilen for assistance with statistical analyses, Queensland Health Forensic and Scientific Services for nutrient analyses, and management and staff at Raptis and Sons for allowing us access to their facilities and regular advice and assistance. We thank 3 anonymous reviewers for their comments. This project was conducted as part of the Tropical Rivers and Coastal Knowledge (TRaCK) program. TRaCK received major funding for its research through the Australian Government's Commonwealth Environment Research Facilities initiative; the Australian Government's Raising National Water Standards Program; Land and Water Australia; the Fisheries Research and Development Corporation and the Queensland Government's Smart State Innovation Fund.

LITERATURE CITED

Adame MF, Reef R, Grinham A, Holmes G, Lovelock CE (2012) Nutrient exchange of extensive cyanobacterial mats in an arid subtropical wetland. Mar Freshw Res 63:457–467

Albuquerque AGBM, Ferreira TO, Cabral RL, Nóbrega GN, Romero RE, Meireles AJA, Otero XL (2014) Hypersaline tidal flats (apicum ecosystems): the weak link in the tropical wetlands chain. Environ Rev 22:99–109

Bayliss P, Buckworth R, Dichmont C (eds) (2014) Assessing the water needs of fisheries and ecological values in the Gulf of Carpentaria. Final Report prepared for the Queensland Department of Natural Resources and Mines (DNRM), CSIRO, Brisbane

Briere PR (2000) Playa, playa lake, sabkha: proposed definitions for old terms. J Arid Environ 45:1–7

Burford MA, Rothlisberg PC, Revill AT (2009) Sources of nutrients driving production in the Gulf of Carpentaria, Australia: a shallow tropical shelf system. Mar Freshw Res 60:1044–1053

Burford MA, Webster IT, Revill AT, Kenyon RA, Whittle M, Curwen G (2012) Controls on phytoplankton productivity in a wet–dry tropical estuary. Estuar Coast Shelf Sci 113:141–151

Chapra SC (1997) Surface water-quality modeling. WCB/McGraw-Hill, New York, NY

Davranche A, Lefebvre G, Poulin B (2010) Wetland monitoring using classification trees and SPOT-5 seasonal time series. Remote Sens Environ 114:552–562

Defries RS, Townshend JRG (1994) NDVI-derived land cover classifications at a global scale. Int J Remote Sens 15:3567–3586

Dortch Q (1990) The interaction between ammonium and nitrate uptake in phytoplankton. Mar Ecol Prog Ser 61: 183–201

Duggan M, Connolly RM, Whittle M, Curwen G, Burford MA (2014) Effects of freshwater flow extremes on intertidal biota of a wet-dry tropical estuary. Mar Ecol Prog Ser 502:11–23

Frazier PS, Page KJ (2000) Water body detection and delineation with Landsat TM data. Photogramm Eng Remote Sens 66:1461–1467

Fry B (2002) Stable isotope indicators of habitat use by Mississippi Delta fish. J N Am Benthol Soc 21:676–685

Greenburg AE, Clesceri LS, Eaton AD (eds) (2005) Standard methods for the examination of water and wastewater, 21st edn. American Public Health Association, Washington, DC

Halpern BS, Walbridge S, Selkoe KA, Kappel CV and others (2008) A global map of human impact on marine ecosystems. Science 319:948–952

Jardine TD, Pusey BJ, Hamilton SK, Pettit NE and others (2012) Fish mediate high food web connectivity in the lower reaches of a tropical floodplain river. Oecologia 168:829–838

Jeffrey SW, Welshmeyer NA (1997) Spectrophotometric and fluorometric equations in common use in oceanography. In: Jeffrey SW, Mantoura RFC, Wright SW (eds) Phytoplankton pigments in oceanography: monographs on

oceanographic methodology, no 10. UNESCO Publication, Paris, p 597–615

Kennard MJ, Pusey BJ, Olden JD, Mackay SJ, Stein JL, Marsh N (2010) Classification of natural flow regimes in Australia to support environmental flow management. Freshw Biol 55:171–193

Kirkwood AE, Henley WJ (2006) Algal community dynamics and halotolerance in a terrestrial, hypersaline environment. J Phycol 42:537–547

Lovelock CE, Grinham A, Adame MF, Penrose HM (2010) Elemental composition and productivity of cyanobacterial mats in an arid zone estuary in north Western Australia. Wetlands Ecol Manage 18:37–47

McFeeters SK (1996) The use of the normalized difference water index (NDWI) in the delineation of open water features. Int J Remote Sens 17:1425–1432

Paling EI, McComb AJ (1994) Cyanobacterial mats: a possible nitrogen source for arid-coast mangroves. Int J Ecol Environ Sci 20:47–54

Paling EI, McComb AJ, Pate JS (1989) Nitrogen fixation (acetylene reduction) in nonheterocystous cyanobacterial mats from the Dampier Archipelago, Western Australia. Aust J Mar Freshw Res 40:147–153

Raven JA (1984) A cost benefit analysis of photon absorption by photosynthetic unicells. New Phytol 98:593–625

R Core Team (2015) R: a language and environment for statistical computing. R Foundation for Statistical Computing, Vienna. www.r-project.org

Redfield AC (1958) The biological control of chemical factors in the environment. Am Sci 46:205–222

Rhodes EG (1980) Modes of Holocene coastal progradation, Gulf of Carpentaria. PhD thesis, Australian National University, Canberra

Ridd P, Sandstrom MW, Wolanski E (1988) Outwelling from tropical tidal salt flats. Estuar Coast Shelf Sci 26:243–253

Ward DP, Hamilton SK, Jardine TD, Pettit NE, Tews EK, Olley JM, Bunn SE (2013) Assessing the seasonal dynamics of inundation, turbidity, and aquatic vegetation in the Australian wet–dry tropics using optical remote sensing. Ecohydrology 6:312–323

Editorial responsibility: Just Cebrian, Dauphin Island, Alabama, USA

Submitted: April 16, 2015; Accepted: January 19, 2016
Proofs received from author(s): February 24, 2016

Estuarine, Coastal and Shelf Science 228 (2019) 106353

Contents lists available at ScienceDirect

Estuarine, Coastal and Shelf Science

journal homepage: www.elsevier.com/locate/ecss

Assessing the distribution and drivers of mangrove dieback in Kakadu National Park, northern Australia

E.F. Asbridge[a,*], R. Bartolo[b], C.M. Finlayson[c,d], R.M. Lucas[a], K. Rogers[a], C.D. Woodroffe[a]

[a] School of Earth and Environmental Science, University of Wollongong, Wollongong, NSW, 2522, Australia
[b] Environmental Research Institute of the Supervising Scientist, Department of the Environment, PO Box 461, Darwin, NT, 0801, Australia
[c] Institute for Land, Water and Society, Charles Sturt University, PO Box 789, Albury, NSW, 2604, Australia
[d] IHE Delft, Institute for Water Education, PO Box 3015, NL-2601, DA, Delft, Netherlands

ARTICLE INFO

Keywords:
Retreat
Colonisation
Sea level rise
Tidal wetlands
Surface elevation
Avicennia marina

ABSTRACT

Satellite observations of Australia's Gulf of Carpentaria between 1987 and 2015 highlighted that many mangroves on the coastline bounding low-lying plains were progressively extending inland and to a lesser extent, in a seaward direction. However, in 2015/16, a significant and widely publicised mangrove dieback event occurred, this was attributed to a combination of climate (temperature, precipitation anomalies) and a ~20–30 cm decline in sea level. A similar but unreported event also occurred in Kakadu National Park (NP) in the Northern Territory. This study aimed to a) quantify the extent of this dieback in the NP, b) establish the characteristics of mangroves (floristics, structure) and the substrate elevation prior to and following event and c) establish links with climate and sea level. Using time-series of high resolution airborne and Unmanned Airborne Vehicle (UAV) data, the majority of mangroves experiencing full or partial dieback were found to occur on the landward margins. Reference to sea-level data indicated that mangroves had colonised and retreated in unison with sea level fluctuations over previous decades but increased in overall extent and cover as sea level rise dominated. Mangroves experiencing full mortality were located on higher elevation substrates where the sea level/tidal influence was least. The study concluded that whilst short-term ENSO-related sea level may result in dieback in northern Australia, the long-term projection of an increase in sea level is anticipated to lead to extension of mangroves in the landward direction.

1. Introduction

Mangroves occur at the interface between the land and the sea and changes to their distribution across floodplains can reflect fluctuations in sea level. Over the past few decades, many mangrove ecosystems in northern Australia have progressively expanded in area, with this documented in time-series of Landsat sensor data from 1987 to 2015 (Asbridge et al., 2016). The incursion of salt water (particularly through networks of tidal creeks) has enabled mangrove to establish and, in some cases, rapidly colonise low-lying basins within many floodplains (Woodroffe et al., 1993). The most spectacular example is the lower Mary River catchment, Northern Territory, where substantial intrusion of saline water into palaeochannels between 1950 and 1990 resulted in expanding tidal creek systems and facilitated the colonisation of mangroves (> 30 km inland extension, predominantly composed of *Avicennia* species) (Knighton et al., 1991; Woodroffe, 1995). However, since the start of the Landsat observation (1987), both seaward and landward extension of mangroves has been observed in many coastal areas, including Kakadu National Park (NP) in the Northern Territory (NT; Asbridge et al., 2015) and the Gulf of Carpentaria in the NT and Queensland (Asbridge et al., 2016). The general extension of mangroves observed up to 2015/16 contrasts with the longer-term pattern of decreasing mangrove extent throughout the late Holocene, which was associated with infilling of tide-dominated estuaries following stabilisation of sea level approximately 7 ka (as determined from pollen analysis; Woodroffe et al., 1985; Woodroffe et al., 1989; Lucas et al., 2018).

In late 2015, fishermen near Burketown in northern Australia became concerned about dieback of mangroves in the Gulf of Carpentaria and the impacts on commercial operations. Satellite-based observations of the mangroves revealed that the dieback was occurring along the landward margin of much of the southern Gulf (Duke et al., 2017; Harris et al., 2018). Field campaigns at locations in northern Australia subsequently established a broader geographic range of mangrove

* Corresponding author.
E-mail address: emmaa@uow.edu.au (E.F. Asbridge).

https://doi.org/10.1016/j.ecss.2019.106353
Received 22 March 2019; Accepted 23 August 2019
Available online 28 August 2019

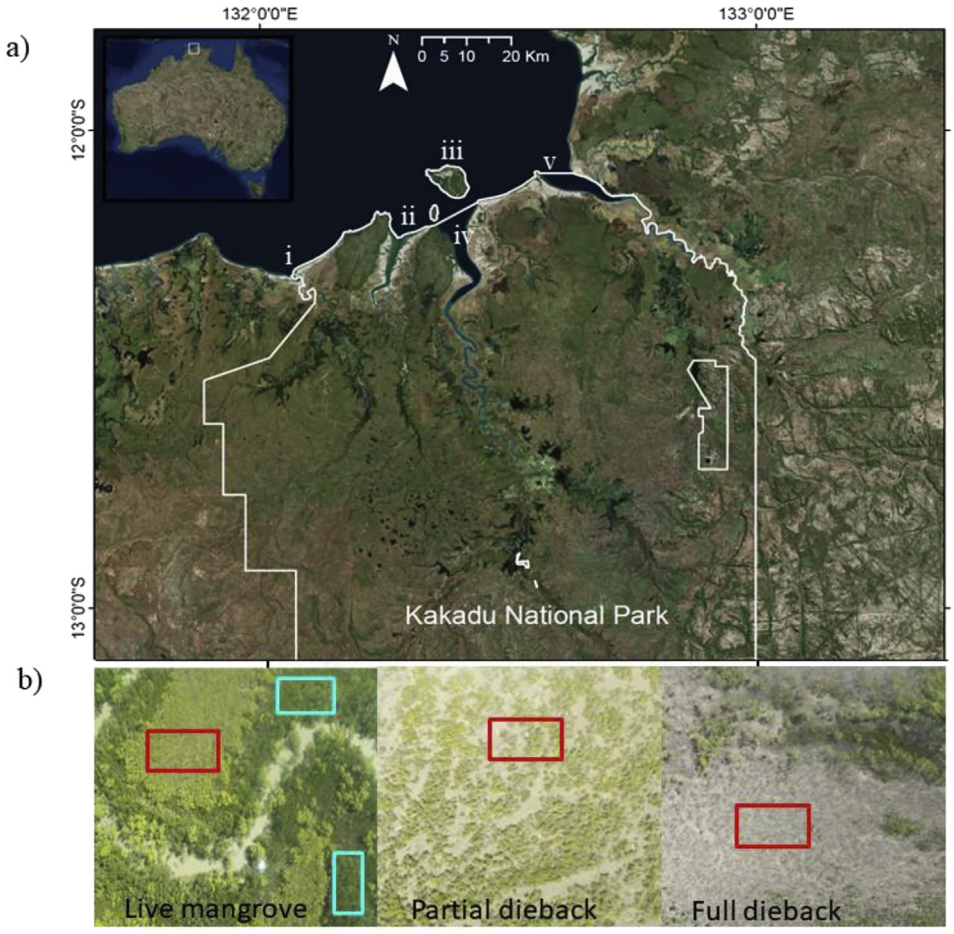

Fig. 1. a: A map of Kakadu NP showing the location of i) the Wildman River, ii) West Alligator, iii) Field Island, iv) South Alligator and v) East Alligator River, b) Examples of aerial drone images used to identify the degree of dieback (live, partial or full), red regions of interest (ROIs) indicate *Avicennia* species and blue ROIs are *Rhizophora* species. (For interpretation of the references to colour in this figure legend, the reader is referred to the Web version of this article.)

dieback including in the World Heritage listed Kakadu NP (Lucas et al., 2018) and Mangrove Bay in Western Australia (Lovelock et al., 2017). The pattern of mangrove dieback was a significant deviation from the consistent trend of mangrove extension along large sections of the north Australian coastline and particularly the Gulf of Carpentaria.

There is increasing support for mangrove extension being related to the interaction between substrate elevation, increasing sea levels and reconnection of low-lying land to the open sea (Asbridge et al., 2016; Asbridge and Lucas, 2016; Woodroffe et al., 2016), as successful mangrove colonisation requires sufficient sediment supply, periodic tidal inundation and sheltered low-lying land free from strong tidal action. Despite understanding the preferential conditions for mangrove colonisation, the cause of recent mangrove dieback remains uncertain. A brief review of possible drivers of change throughout the Gulf of Carpentaria (Harris et al., 2018) highlighted unusually low sea levels, elevated salinity levels, low rainfall, below average vapour pressure and above average temperatures. In Kakadu NP, the dieback was linked to anomalously low sea level in the region over the dieback period, as measured from satellite altimetry, and which contrasted to global patterns of increasing sea levels (Lucas et al., 2018). The dieback also coincided with a period of higher than average air temperatures and weakening of the monsoon, which corresponded with negative phases of the El Niño Southern Oscillation (ENSO) and positive phases of the Indian Ocean Dipole (IOD). In Mangrove Bay, two canopy dieback events were observed in 2002/2003 and 2015/2016 respectively (Lovelock et al., 2017), with the latter being more extensive and coinciding with the dieback observed in the Gulf of Carpentaria and Kakadu NP. The mean annual sea level measured at Exmouth, the nearest tide gauge site, indicated that both events were related to a reduction in sea level and a 25–30% increase in pore water salinity. From 2000 to 2016, the change in annual and seasonal rainfall did not show a significant correlation with soil pore water salinity, indicating that rainfall may have very little influence on salinity stress experienced by the mangroves. Variations in the Landsat-derived Normalised Difference Vegetation Index (NDVI) indicated greatest variation with distance from the river mouth and in the inland sections of the creeks, thereby suggesting that the mangroves furthest from exposure to the incoming tide will be less frequently inundated during the high tide and are at a higher risk of dieback (Lovelock et al., 2017). Evidently, the coincidence of a range of possible drivers is limiting attribution of the primary cause of the change.

Given that the recent spatial pattern of landward mangrove extension throughout many areas of Northern Australia has been attributed to the interaction of sea-level fluctuations and other geomorphological processes (Asbridge et al., 2016; Asbridge and Lucas, 2016), we postulated that the spatial pattern of mangrove dieback and the structural character of the affected vegetation may provide an indication of underlying causes. More specifically, we hypothesised that the recent and temporary decline in sea level documented from satellite altimetry in northern Australia would largely influence landward mangroves that had previously extended following a prior period of sea-level rise. Accordingly, the impacted trees should be positioned at higher positions within the tidal frame and of shorter stature due to the combined effects of younger tree ages and less suitable edaphic conditions. Building upon comprehensive analyses of mangrove distribution dynamics in Kakadu NP (Asbridge and Lucas, 2016; Lucas et al., 2000, 2002, 2018; Woodroffe, 1995; Woodroffe et al., 1989), the aim of this study was to determine local drivers of expansion within areas that had experienced dieback in the context of broader climate and sea-level change. To address the aim, the objectives were to use combinations of spectral

indices derived from high (< 6 m) spatial resolution airborne and satellite sensor data and Light Detecting and Ranging (LiDAR) data to:

a) Quantify and describe different states (structure, floristic composition) of mangrove prior to and in 2014 and 2016 to determine the locations and magnitudes of dieback.
b) Establish the three-dimensional elevation of the underlying substrate associated with different mangrove communities and dieback condition.

2. Materials and methods

2.1. Study site

The climate in Kakadu NP is composed of a wet and dry season, with majority of the rain (90%) in the wet season, with annual rainfall intensities reaching 100 m per hour (Finnegan, 1993). The rainfall is associated with monsoonal troughs over Southeast Asia, yielding a mean annual rainfall of 1300 mm to 1500 mm (McQuade, 1993). The temperature is cooler in the dry season (minimum 17 °C to maximum 32 °C) and warmer in the wet season (24 °C–34 °C). Within Kakadu NP, mangroves are located primarily along the coastal margins of the tide-dominated estuaries of the East, South and West Alligator and Wildman Rivers and Field and Barrow Islands (Fig. 1a). The most extensive and tallest (~20–25 m) mangroves are located along the banks and towards the mouth of the West Alligator River. Zonation is common, with *Rhizophora stylosa* occupying the central intertidal zone with *Sonneratia alba* and both *Ceriops tagal* and *Avicennia marina* dominating the seaward and landward mangrove zones respectively in varying proportions. *A. marina* is the most widespread throughout the intertidal zone, occurring as a pioneering tree on the seaward margin and as largely monospecific shrubland on the landward margin (extending up the estuary towards the tidal limit; Finlayson and Woodroffe, 1996; Lucas et al., 2018; Woodroffe, 2018).

2.2. Remote sensing and ground data

Over the past few decades, a number of campaigns have been conducted to capture airborne remote sensing data over Kakadu NP. These include true colour stereo aerial photographs (frame size of 230 × 230 mm) acquired in 1991 using a Wild CR10 flying at 3962 m (Mitchell et al., 2007). Over 100 photographs were taken and, using procedures outlined by Lucas et al. (2002), were orthorectified and merged into separate mosaics for each of the major rivers and islands. Hyperspectral Compact Airborne Spectrographic Imager (CASI) data were also acquired in 2002, for the West Alligator River, at 1 m resolution. Between October and November 2011, airborne LiDAR (Leica ALS60) data were acquired over the same area and, from these, 2 m spatial resolution Digital Terrain Models (DTMs) and Canopy Height Models (CHMs) were generated. Given the advancement in geo-referencing of LiDAR, each of the 1991 orthomosaics were later georeferenced to the LiDAR data using only ground control points associated with landscape features that were considered unchanged within the landscape between 1991 and 2011.

Between 6 and 7 September 2016, multispectral visible, red edge and near infrared images were acquired at a spatial resolution approximating 10 cm from a micasense sensor on-board a Swampfox fixed wing drone. Subsequently, the sensor was attached to an R44 helicopter and transects were flown at an elevation of approximately 70 m. Eight sites along the Wildman and West Alligator River were targeted, with these associated with areas experiencing significant colonisation by mangroves (see Asbridge and Lucas, 2016). The sensor also provided the capacity for stereo imaging and hence retrieval of mangrove CHMs. A second airborne overflight over the East, South and West (east bank) Alligator Rivers, the Wildman River and both Field and Barrow Islands was undertaken on 8 September 2016, using a CESSNA aircraft, with colour photographs taken obliquely from both sides. All photographs used in the study were mapped onto Google Earth Imagery to determine their geographic footprints.

For Kakadu NP, RapidEye data were provided through Planetlabs Ambassador Program for 2014 (pre-dieback) and 2016 (post-dieback) respectively at a nominal spatial resolution of 6.5 m (Planet, 2017; Figure A1), with all scenes atmospherically corrected using ARCSI (Bunting et al., 2018) and tiled using RSGISLib software (rsgislib.org).

Within these data, mangrove zones dominated by different species were particularly distinct in the near infrared, red edge and blue composite images. From each, the NDVI and Plant Senescence Reflectance Index (PSRI) were calculated, with these selected because of sensitivity to green and dead components of vegetation respectively. The NDVI is sensitive to vegetation productivity, with values ranging from −1.0 to 1.0, whist the PSRI is sensitive to carotenoid accumulation or retention in leaves experiencing senescence (Merzlyak et al., 1999). An increase in PSRI is correlated to an increase in canopy stress and the start of senescence, indicated by an increase in carotenoids in relation to the chlorophylls. PSRI values range from −1 to 1, with green vegetation usually between −0.1 and 0.2. The PSRI has been used to indicate mangrove physiological stress (Clewley et al., 2014; Flores-de-Santiago et al., 2013; Lucas and Mitchell, 2017; Muhsoni et al., 2018).

2.3. Previous maps of mangrove extent

Mangrove extent and change had been mapped previously from the 1991 orthomosaics and 2011 LiDAR data by Asbridge and Lucas (2016). To summarise, the 1991 orthomosaics (post-referenced to the 2011 LiDAR) were individually segmented (with each segment typically comprised of < 50–100 1 m^2 pixels for mangroves) and the broad area of the different cover types (mangroves, mudflats, water, woodlands) was classified by applying a maximum likelihood algorithm within the Environment for Visualizing Images (ENVI) software. The classification was then refined by methodically examining each segment (and particularly those at the margins of the mangroves) and re-assigning incorrectly classified segments based on visual interpretation and identification. The reassignment was based on the dominant land cover within each segment. Mangrove extent in 2011 was determined by identifying all vegetated areas with a CHM elevation of ≥0.5 m and removing areas of non-mangrove (primarily woodlands, which had remained largely unchanged) by referencing the 1991 orthomosaics and Google Earth Imagery. Losses and gains in mangroves over the 20-year period (1991–2011) were then quantified by comparing extents for each year. The resulting maps of change indicated little variation in net mangrove area. However, there was considerable redistribution with significant losses and gains of mangrove due to progressive inland intrusion along many of the smaller creeks and localised seaward expansion (particularly along the western mouth of the West Alligator River). Mangrove loss was evident along some coastal margins and inland creeks. Seaward losses could be associated with the processes of erosion, storm damage and, to a lesser extent, lightning strikes. Gains were attributed to sediment accretion linked to periods of greater river discharge (leading to increases in freshwater inundation and localised sea level) and saline intrusion as a consequence of progressive, albeit fluctuating, rises in sea level.

2.4. Mapping mangrove extent and dieback (2014 and 2016)

Using the 2014 RapidEye data, the coastal boundary of Kakadu NP was redefined for the purpose of this study as the river morphology had changed in some areas, particularly along the Wildman River. The area of mangroves in Kakadu NP was then re-calculated and used as a basis for determining the proportion of mangroves that had experienced full or partial dieback or had remained alive.

Mitchell et al. (2007) only mapped the extent of mangroves in 1991 along the mouths of the major rivers and along the coastlines and hence

no maps were available for the upstream sections. For this reason, a revised mangrove map for Kakadu NP was generated for 2014 (prior to the dieback event) with reference to 5 m RapidEye (Planet, 2017) visible, red edge and near infrared data (orthorectified, atmospherically corrected and combined within a single mosaic). The mapping was guided by the existing map of Hay et al. (2005) (for the nominal year of 2000) which was generated for northern Australian mangroves from Landsat Thematic Mapper (TM) imagery using the technique outlined in Danaher (1995). Whilst the 2000 map provided a good indication of where mangroves might be located, the spatial resolution of the Landsat sensor was ~30 m and many of the smaller areas of mangroves (particularly in the upstream sections) were not captured (with this partly attributed to changes occurring since 2000). Nevertheless, the data provided an indication of potential mangrove areas and was therefore used as a broad mask (encompassing other proximal land covers) to provide a focus for more detailed mapping.

To classify mangroves as well as other vegetation (e.g. samphires, Eucalyptus woodlands), mudflats, and both turbid and relatively clear water observed within the masked area of the 2014 RapidEye data, a maximum likelihood algorithm was applied. Training statistics were extracted from > 200 regions of interest (ROIs) for each class, with these identified with reference to combinations of Google Earth Imagery, Landsat sensor data, 1991 aerial imagery, 2002 CASI data and 2011 LiDAR data as well as drone visible (RGB) imagery and ground data (with the latter acquired in September 2016). The accuracy of the classification of the 2014 image was not assessed, as there were no time coincident ground data. However, accuracy was estimated for the 2016 classification (including areas of dieback; see later sections) and using > 200 ROIs identified from the range of imagery outlined above and reserved for testing. Following mapping of mangrove extent for 2014, the equivalent area within the 2016 RapidEye image was extracted.

ROIs were drawn over sections of the forest observed as being either dead, partially dead or live in 70 aerial drone images acquired at the mouth of the West Alligator River during the field campaign in September 2016 (Fig. 1b) and for which the dominant genus could be identified from the 2014 RapidEye composite images. From each area, all PSRI and NDVI values for 2014 and 2016 were extracted as well as the NDVI and PSRI difference. These data were then used to define thresholds for differentiating different conditions of dieback classified as living, partial or dead. The resulting thresholds were then used to determine the area of extent of full or partial dieback across all mangroves in Kakadu NP. To validate the dieback condition maps, additional ROIs were defined using the drone images as well as oblique aerial photographs taken from a Cessna aircraft during an overflight (7 September 2016).

2.5. Drivers of change

For each year between 1987 and 2015, changes in the extent of mangroves as a function of cover, were previously quantified for the West Alligator River by Asbridge and Lucas (2016). With the exception of 2010 and 2012, where data were affected by cloud cover and the Landsat-7 sensor error). An estimate of Foliage Projective Cover (FPC) was generated annually and mangrove occurrence was assigned to all pixels with an FPC > 30% within a predefined mask (to exclude other vegetation). In this study, the FPC was extracted from all pixels associated with full or partial dieback between 1987 and 2014.

Asbridge and Lucas (2016) and Asbridge et al. (2016) established a link between mean sea level changes and mangrove extent but at the time, did not explore the relationship with El Niño intensity. An indicator of intensity is the Nino 3.4 index, which is used to classify ENSO conditions over the Pacific Ocean and is derived from satellite altimetry data from 1993 onwards, including for the Arafura Sea and Timor Sea (NOAA/NESDIS/STAR Laboratory for Satellite Altimetry, 2018). The mean sea level and Nino 3.4 data were summarised to a single value for each year so as to determine the influence of both on changes in annual mangrove extent for the years that satellite altimetry data were available (i.e., 1993 onwards). Lucas et al. (2018) suggested that there was a lag of approximately 2 years between the time of mangrove establishment and detection of a vegetation signal within the Landsat sensor data and hence this time offset was added to account for the time needed for mangroves to establish a cover or adjust. This delay was also considered appropriate for quantifying the effects of El Niño intensity on mangrove condition. For this, a two-way Analysis of Variance (ANOVA) was performed, with each year included in each model to account for spatial autocorrelation in mangrove extent dynamics. A full factorial ANOVA was subsequently undertaken to establish whether all factors contributed to understanding of changes in mangrove extent and where refinement of the model might be achieved.

2.6. Spatial pattern and structural character of mangrove dieback

Estuary geomorphology and the interaction of tide, wave and river energy can have a profound effect on tidal currents as they propagate along estuaries (Dalrymple et al., 1990). The vertical distribution of mangroves with respect to a height datum will also vary according to changes in the tidal prism and river flow. Accordingly, tidal energy is less impeded on a coastal plain and rises to a maximum near the entrance of infilled estuaries before dissipating in a landward direction due to frictional dissipation (Heap et al., 2004). In this study, the variable effect of tides on the vertical distribution of mangroves throughout Kakadu NP was accounted for by differentiating pixels on the basis of whether they were associated with the landward estuarine or seaward coastal floodplain (Woodroffe, 2018) and subsequently associating these with a dieback condition (i.e., full or, partial dieback or live, as determined from the temporal analysis of RapidEye data).

To test the hypothesis that a recent fall in sea level would preferentially influence mangroves at higher elevation, the elevations of each live, partially dead and fully dead cell were first extracted from the 2 m LiDAR-derived DEM for the West Alligator River. A two-way ANOVA was then used to test for significant differences between dieback condition and floodplain position (i.e., estuarine or coastal), with a post-hoc Tukeys HSD conducted to establish relative significance between variables. These same tests were also used to establish whether flood plain position, mangrove dieback condition and stand height (to the nearest m) determined from the 2 m LiDAR-derived CHM were related.

3. Results

3.1. Pre-dieback mangrove extent

Based on the revised mapping of mangroves in Kakadu NP from 2014 RapidEye data (Fig. 2), the total area of mangrove was estimated at 183.4 km^2, with this representing 0.96% of the total national park area (19,144.0 km^2). In contrast to previous mapping efforts (Mitchell et al., 2007; Asbridge and Lucas, 2016), the mapping captured mangroves in the upper reaches of the Wildman, West, South and East Alligator Rivers, was at a higher spatial resolution compared to Hay et al. (2005) and updated to 2014. The map is also available through the Terrestrial Environment Research Network (TERN) Landscapes data portal.

3.2. Observations of mangrove dieback

Many of the creeks that are known to be experiencing inland intrusion of saltwater, maintained full canopy cover. This was particularly noted along the eastern mudflats of the West Alligator River (Fig. 3a) where an intricate network of creeks has been progressively developing over the past few decades. From observations from the CESSNA, mangroves were in good condition across most of Field Island

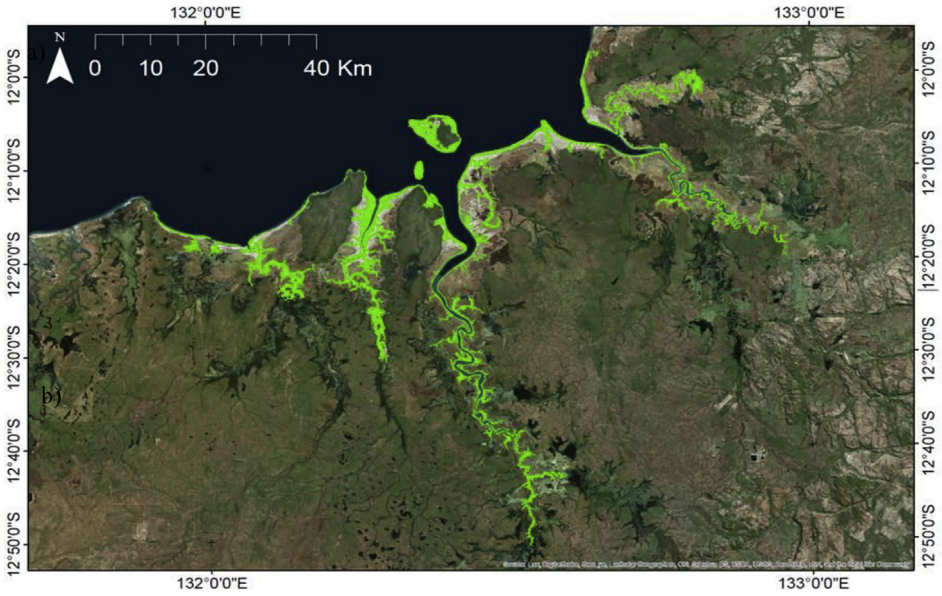

Fig. 2. The extent of mangroves in 2014 in Kakadu NP generated through classification of RapidEye data.

and along much of the East Alligator River. Along the West Alligator River, mangroves forming the seaward zone and dominated by *S. alba* and *R. stylosa* remained healthy, but significant dieback was observed within the inland zone dominated by *A. marina* (although interspersed by *S. alba*). Many of the trees affected were of lower stature (typically < 5–8 m in height) and located on the landward margins (Fig. 3b, c, d and e). Further dieback was observed in the very upper reaches of creeks (Fig. 3f and g), which were previously identified as hotspots for mangrove inland colonisation.

Dieback was also observed along sections of the East, South Alligator and Wildman Rivers. On Flying Fox Island, located within the mouth of the East Alligator River, many of the larger trees had died,

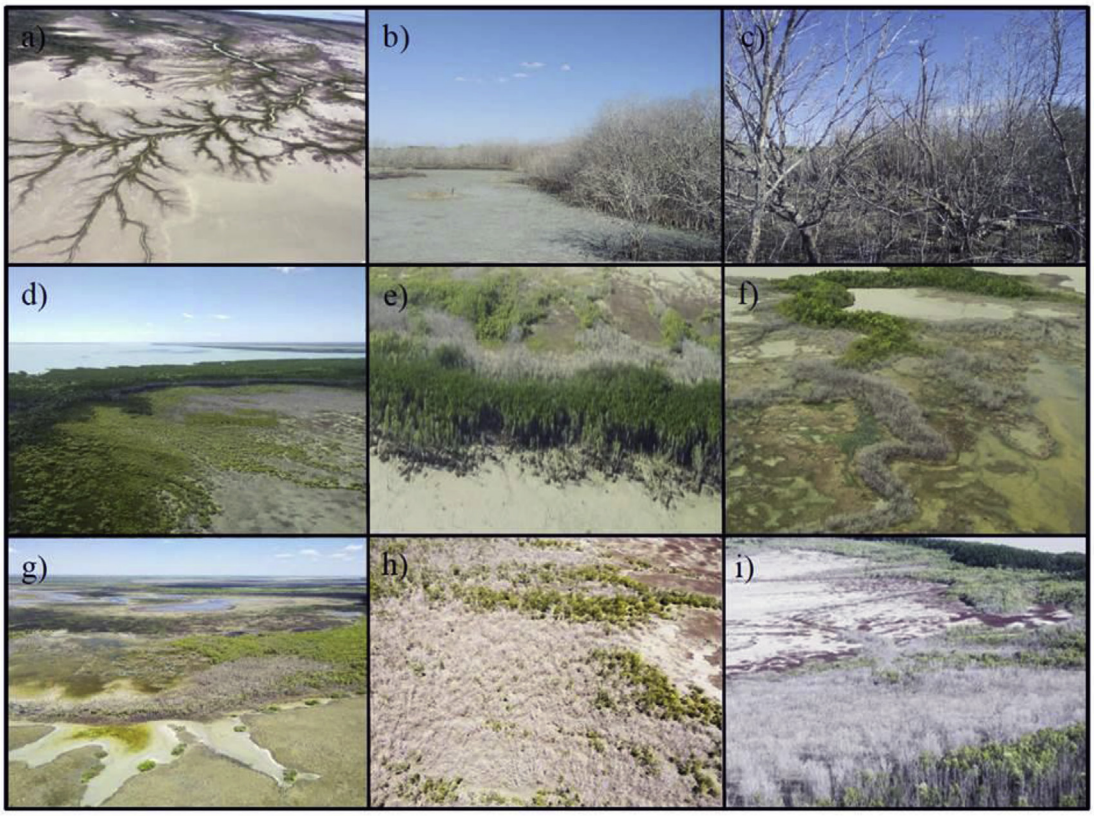

Fig. 3. West Alligator - a) Mangrove colonisation along eastern creeks, with no dieback observed; b, c, d and e) examples of dieback along the landward side; f and g) dieback occurring in the upper reaches of tidal creeks, where mangroves were previously experiencing landward extension primarily due to sea-level rise. Mangrove dieback observed along the banks of the h) East Alligator River, and i) the Wildman River, predominantly within the landward mangrove stands and along the more distal sections of tidal creeks.

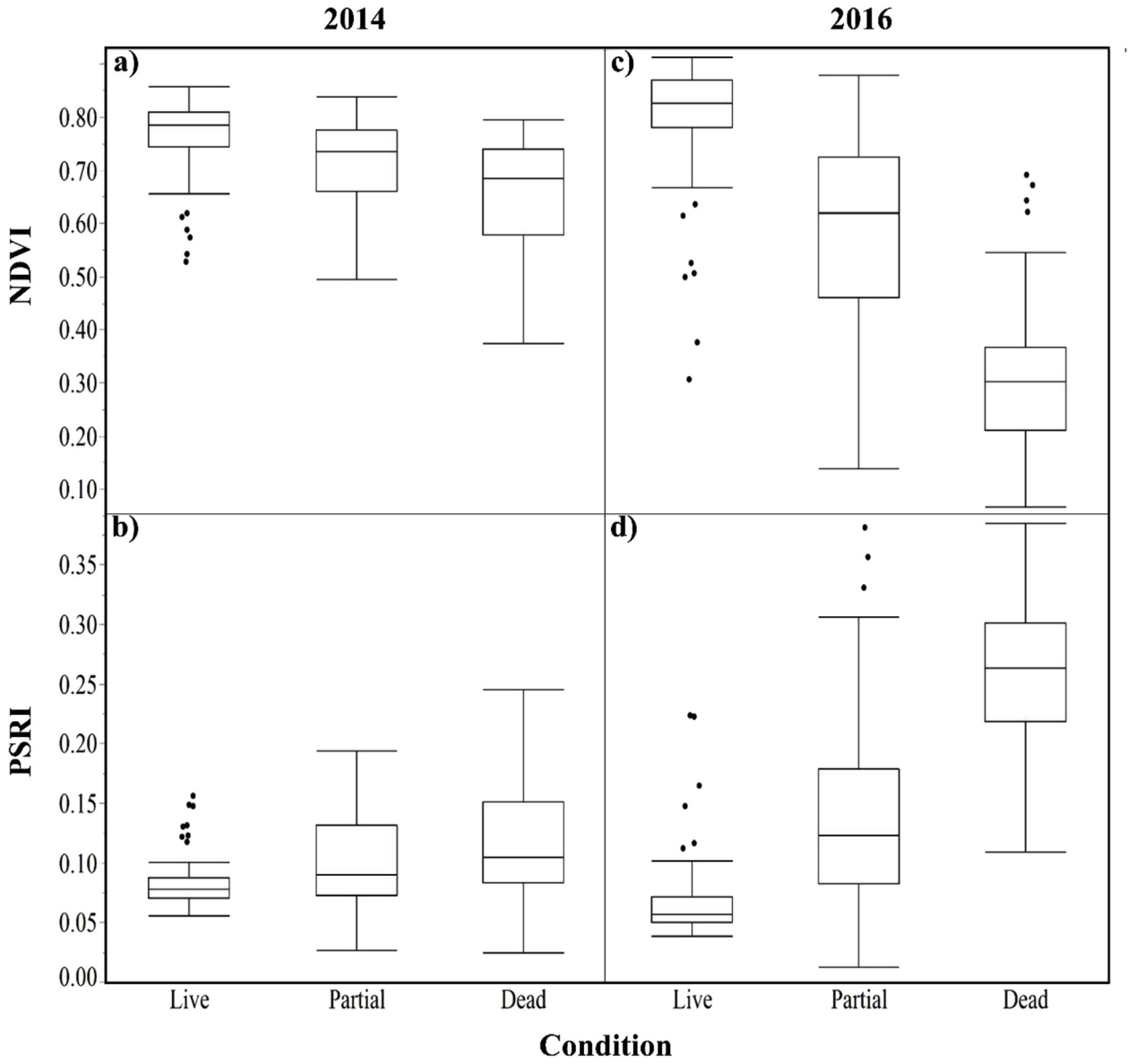

Fig. 4. Box and whisker plots of the RapidEye NDVI and PSRI of mangroves prior to (in 2014) and following (2016) the dieback event in 2015/16, *differentiating* between dead, partially dead and live (green) mangroves.

with large patches experiencing full or partial mortality (Fig. 3h). Similarly, smaller separated sections of taller mangroves were also dead in the South Alligator River. Extensive dieback was also observed along the Wildman River with many tall dead *A. marina* trees, particularly on the landward margins, contrasted with the other tree species that had survived (Fig. 3i). The Wildman River mangroves had previously experienced significant damage from storm events, including Cyclone Monica (20th to 28th April 2006), although these had recovered at the mouth during the post-storm period.

3.3. Detection of dieback condition

Frequency statistics of the NDVI and PSRI extracted from mangroves prior to and following the dieback event in 2015/16 highlighted the benefit of integrating these indices (Fig. 4). For mangroves living prior to the event (i.e., in 2014), the NDVI and PSRI were 0.60–0.83 and 0.07–0.135 respectively (based on the upper (25%) and lower (75%) quartiles). However, the NDVI and PSRI were lower and higher respectively for those mangroves that subsequently experienced dieback suggesting that both might be used to warn of a forthcoming event. In areas experiencing full dieback, the NDVI decreased to 0.2–0.35 and the PSRI increased to 0.22–0.3 but these changes were comparatively less for mangroves with partial dieback. Mangroves that experienced complete mortality by 2016 had a lower NDVI and a higher PSRI in 2014 compared to those that remained alive or experienced partial mortality. This was attributed to these mangroves only recently colonising the landward margins and hence were generally smaller in stature and more sparsely distributed (i.e., with a reduced overall canopy density) compared to the more established trees which had experienced partial or no mortality.

Whilst the NDVI and PSRI were considered useful for differentiating dieback condition, the NDVI difference provided greatest separability. On the basis of the overlaps between the frequency histogram, dead, partially dead and live mangroves were associated with the NDVI difference ranges of > 0.5 (equating to a change from 0.6 to 0.1), < 0.5–0.1 and < 0.1 respectively. The NDVI difference between 2014 and 2016 overlain onto the 2011 LiDAR-derived DTM is given in Figure A2 for the West Alligator River, with the greatest extent of dieback evident towards the landward margin and for mangroves dominated by *A. marina* (as determined from the RapidEye composite).

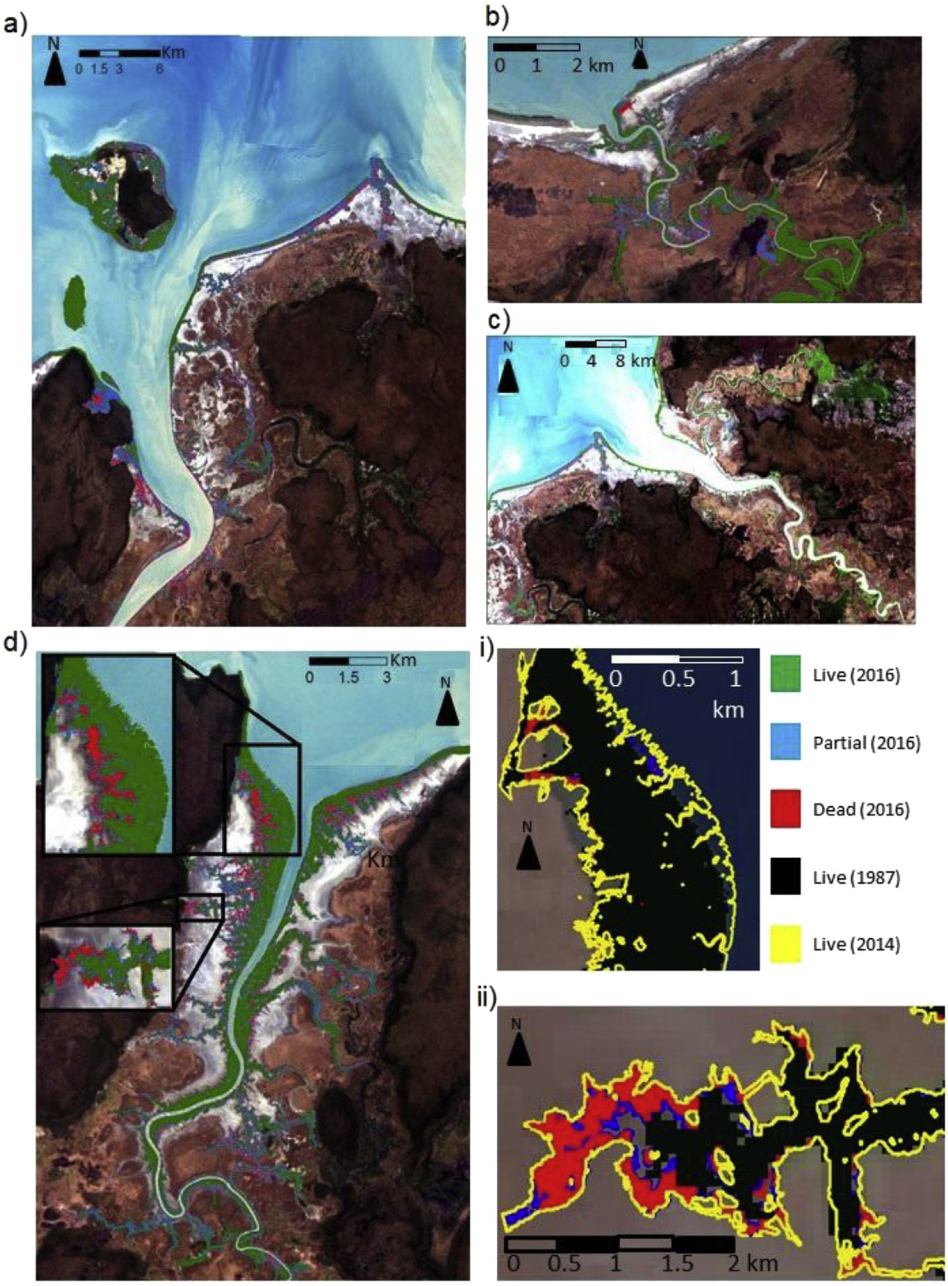

Fig. 5. The extent and dieback condition of mangrove forests along a) South Alligator River, including Barrow Island and Field Island b) Wildman River c) East Alligator River and d) West Alligator River following the 2015/2016 dieback event. The latter indicates the spatial differences in the age and structure of mangroves experiencing dieback at the i) river mouth and ii) the uppermost sections of small creeks.

Increases in the NDVI were evident but small in comparison to the area of decrease. On this basis, the NDVI difference was used to map the extent of dieback across Kakadu NP (Fig. 5).

As conveyed in Fig. 5d, the majority of the mangrove dieback in Kakadu NP was found along the landward margins where *A. marina* was dominant. Forests dominated by *Sonneratia* and *Rhizophora* species along the seaward margin and central zones were not affected. Significant dieback of *Avicennia* and some *Sonneratia* species was also observed in the upper reaches of the creeks that were previously identified as experiencing long-term saltwater intrusion (Asbridge and Lucas, 2016).

The maps of the extent of mangroves and the different dieback conditions indicated that majority of the dieback occurred on the landward margins, with the majority on the West Alligator River colonising between 1987 and 2014. Those towards the seaward margin of this catchment (with the exception of a newly colonising fringe on recently accreted sediments) were present throughout the period of the time-series.

Based on the NDVI difference thresholds, the area of full and partial dieback across Kakadu NP in 2016 was estimated at 10.4 km^2 and 16.5 km^2 respectively, with this equating to approximately 17.5% for each of the Wildman and West and South Alligator River mangroves and between 7.0% and 8.4% of Field Island and East Alligator River mangroves (Table 1). The total area affected was 25.9 km^2 or 14.7%.

The accuracy of mapping of mangrove dieback condition for the West Alligator River, based on the interpretation of the available drone data, was 77%, with Users' and Producers' accuracies ranging from 70.6 to 82.1% and 46.3–75.0%. The lower Producer's accuracy for partial dieback was attributed to the wide range of NDVI difference values and proportions of the canopy affected which could not be quantified

Table 1
The area of mangroves in Kakadu NP associated with different dieback condition.

Location	Total (km^2)	Live (km^2)	Partial dieback (km^2)	Full dieback (km^2)	Partial dieback (%)	Full dieback (%)	Total affected (%)
Wildman River	21.6	17.8	2.3	1.5	10.6	6.9	17.6
West Alligator River	51.1	42.4	5.3	3.4	10.4	6.7	17.0
South Alligator River	58.3	48.0	6.3	4.0	10.8	6.9	17.7
Field Island	20.2	18.8	0.9	0.5	4.5	2.5	6.9
East Alligator River	32.2	29.5	1.7	1.0	5.3	3.1	8.4
TOTAL	183.4	156.5	16.5	10.4	9.0	5.7	8.0

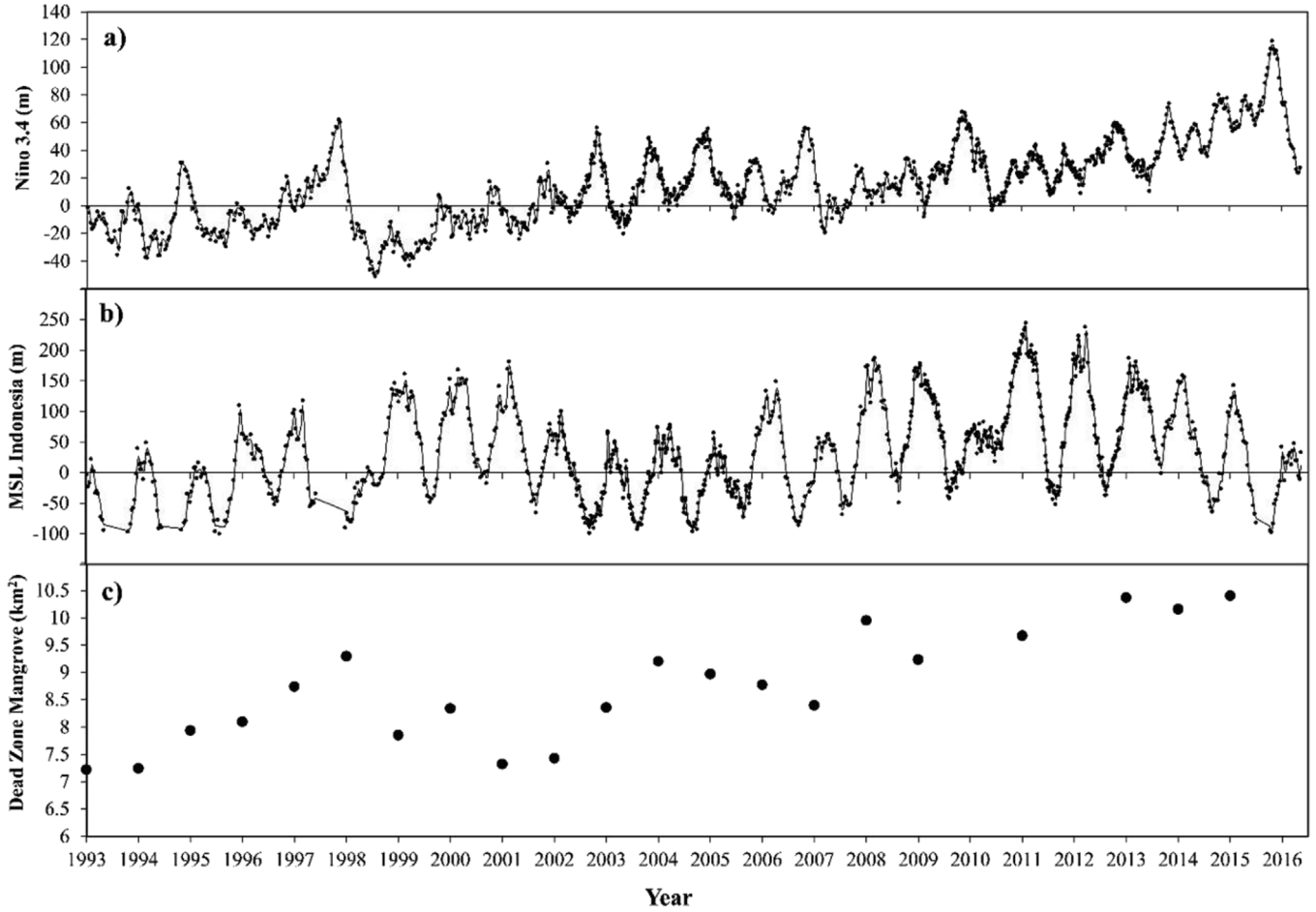

Fig. 6. a) El Niño intensity, as indicated by Nino3.4 from satellite altimetry, b) mean sea level derived from satellite altimetry mean sea level product for the Indonesian region, and c) mangrove extent within the landward dead zone mangrove mapped in 2016 (NB: lag in extent was not applied to this figure and mangrove extent is based on what was classified from remote sensing imagery. Accordingly, the extent of mangrove in this dead zone in 2016 was 0 km^2).

consistently from the drone imagery because of the diverse spatial patterns and complex geometric configurations of dieback. For the remaining rivers and islands, overall accuracies ranged from 75.0 to 89.7%.

3.4. Drivers of mangrove landward expansion

Changes in the extent of mangrove within the landward zone and experiencing dieback in 2016 exhibited a strong and significant positive relationship with mean sea level (Fig. 6b and c; $r^2 = 0.72$, $p = 0.0002$). Effect tests indicated a strong influence of spatial autocorrelation on mangrove expansion (i.e., Year: $p = 0.0002$). However, a significant interaction effect with mean sea level ($p = 0.0298$) demonstrated the role of changes in this variable in promoting mangrove expansion and subsequent decline in the landward zone (Table 2). Whilst the model incorporating Nino3.4 was significant ($r^2 = 0.69$, $p = 0.0005$), the effect tests did not demonstrate a significant contribution of Nino3.4 to mangrove distribution dynamics (Table 2, Fig. 6a). The coefficient of determination was only marginally improved when incorporating mean sea level and Nino3.4 within a full factorial ANOVA ($r^2 = 0.77$, $p = 0.0066$).

3.5. Spatial pattern and structural character of mangrove dieback

Approximately 20% of cells were found to be either fully or partially impacted by dieback (n = 291266), with a greater proportion associated with the estuarine (15%) than the coastal plain (5%; Table 3). The mean elevation (above mean sea level; msl) of living, partial and dead mangrove was 2.11 m, 2.35 m and 2.38 m respectively (Table 3), and differences in elevations based on dieback condition were significant ($p < 0.0001$). The least squares mean of the model incorporating both dieback condition and mangrove position indicated

Table 2
Results from ANOVAs modelling the effect of mean sea level changes and El Niño intensity, indicated using Nino3.4 data.

Model	ANOVA					Effects Test				
	Source	DF	SS	MS	F Ratio	Effect	DF	SS	F Ratio	Prob > F
MSL x Year	Model	3	11.85	3.95	13.38	Year	1	6.79	23.01	0.0002
	Error	15	4.43	0.30	**Prob > F**	MSL	1	0.78	2.63	0.13
	C. Total	18	16.28		0.0002	Year x MSL	1	1.70	5.76	0.0298
Nino3.4 x Year	Model	3	11.16	3.72	10.89	Year	1	0.97	2.85	0.11
	Error	15	5.12	0.34	**Prob > F**	Nino3.4	1	0.61	1.78	0.20
	C. Total	18	16.28		0.0005	Year x Nino3.4	1	1.09	3.21	0.09
MSL x Nino3.4 x Year	Model	7	12.64	1.81	5.46	Year	1	0.98	2.95	0.11
	Error	11	3.64	0.33	**Prob > F**	Nino3.4	1	0.072	0.22	0.65
	C. Total	18	16.28		0.0066*	Year x Nino3.4	1	0.00	0.00	0.95
						MSL	1	0.10	0.29	0.60
						Year x MSL	1	0.22	0.67	0.43
						MSL x Nino3.4	1	0.66	2.01	0.18
						Year x MSL x Nino3.4	1	0.00	0.00	0.98

SS = Sum of squares; MS = Mean square.

Table 3
The number of pixels classified as living, partially impacted or dead within Kakadu NP, the coastal plain and estuarine plain, mean elevation and height of pixels and the least squares mean (LSM) height and elevation of living, partial and dead pixels on the coastal and estuarine plain.

		Living	Partial	Dead
Number of pixels (n) (% of total)	West Alligator River	233 197 (80)	32469 (11)	25600 (9)
	Coastal plain	43165 (15)	5892 (2)	7487 (3)
	Estuarine plain	190 032 (65)	26577 (9)	18113 (6)
Elevation (m)	Mean	2.11	2.35	2.38
	LSM Coastal plain	1.54	2.32	2.37
	LSM Estuarine plain	2.24	2.36	2.38
Height (m)	Mean	6.67	2.42	2.38
	LSM Coastal plain	8.74	3.52	2.62
	LSM Estuarine plain	6.20	2.18	2.28

that elevations on the coastal plain were lower than that on the estuarine plain for each dieback condition and these differences significant ($p < 0.0001$). A post-hoc analysis indicated that there was little difference between the elevations of dead mangrove, irrespective of dieback condition (Fig. 7). Furthermore, mangroves experiencing full or partial dieback were of significantly lower stature compared to those that remained alive ($p < 0.0001$, Table 3), and that this relationship was modulated based on whether the mangrove were associated with the coastal or estuarine plain (Fig. 7). Post-hoc analysis indicated little difference in the heights of dead and partial dieback condition on the estuarine plain (Fig. 7). The tallest mangrove were associated with lower elevations on the coastal plain and these mangrove were the least likely to be impacted by dieback, whilst the shorter mangroves, located at higher elevations on either the coastal or estuarine plain were more vulnerable to dieback.

4. Discussion

4.1. Mangrove dieback and causes

The 2015/2016 dieback event observed in Kakadu NP coincided with large-scale dieback events across the Gulf of Carpentaria where an estimated 7400 ha (6%) of the mangroves experienced mortality. At the time of the investigation by Duke et al. (2017), the dieback event in the Gulf of Carpentaria was thought to be unprecedented in terms of the extent and severity. Our investigation in Kakadu NP and others (Lovelock et al., 2017), demonstrates that the 2015/2016 dieback event was not confined to the Gulf of Carpentaria, with full and partial dieback in Kakadu NP in 2016 estimated at 10.4 km^2 and 16.5 km^2 respectively, comprising 14.7% of the total area of mangrove. The areas experiencing partial and complete dieback, varied between rivers, with the Wildman River, West and South Alligator catchments affected more (~17.5%) compared to the East Alligator River (8.4%) and Field Island (6.9%).

For most of the rivers within Kakadu NP, dieback of mangroves was most evident along the landward margins. Historic changes in mangrove extent from 1987 to 2014 indicate that the trees experiencing mortality in 2015/2016 were previously the young (approximately 1–5 years old) newly colonising trees extending landward along the creeks (Asbridge and Lucas, 2016). (Fig. 5). The most extensive area was on the western bank of the West Alligator River where mangroves dominated by *A. marina* had suffered complete mortality and those remaining showed evidence of fungal infections (leaf loss, leaf spots and trunk rot) and leaf deformations (smaller irregularly shaped leaves) (Asbridge and Lucas, 2016 *pers. obs.*). Mangroves on the eastern bank were less affected and appeared to be thriving on the upper reaches of the creeks, and were continuing to extend inland. Mangroves occurring on the other rivers and towards the seaward margins were generally less affected. Even so, large patches of dieback were observed, including within taller forests which suggests other processes may be exerting an influence on vitality, perhaps localised elevation changes. In contrast to the Gulf of Carpentaria, continuous sections exceeding several 10s of kilometres were not identified, with the exception of the West Alligator River where continuous mangrove (approximately 10–15 km) on the landward side of the west bank (estuarine section) and east bank (coastal section) had experienced dieback.

The dieback was largely confined to monospecific stands of *A. marina* on the landward margin, as opposed to the taller *Rhizophora* and *Sonneratia* species, which were largely unaffected. The differential degree of impact between species was related to the distribution of species along tidal gradients that reflect species-specific tolerance to salinity and inundation, as well as the longer period of site occupation of *Rhizophora* and *Sonneratia* and more recent expansion of *A. marina*. The finding that *A. marina* exhibited greater impact is surprising as the species is often cited as a pioneer with tolerance to a wide range of conditions, including drought, high temperatures (upper limits of tolerance for air temperature: 35.6 °C and sea surface temperature: 32.8 °C (Quisthoudt et al., 2012),) and high salinities (Khan and Aziz, 2001;

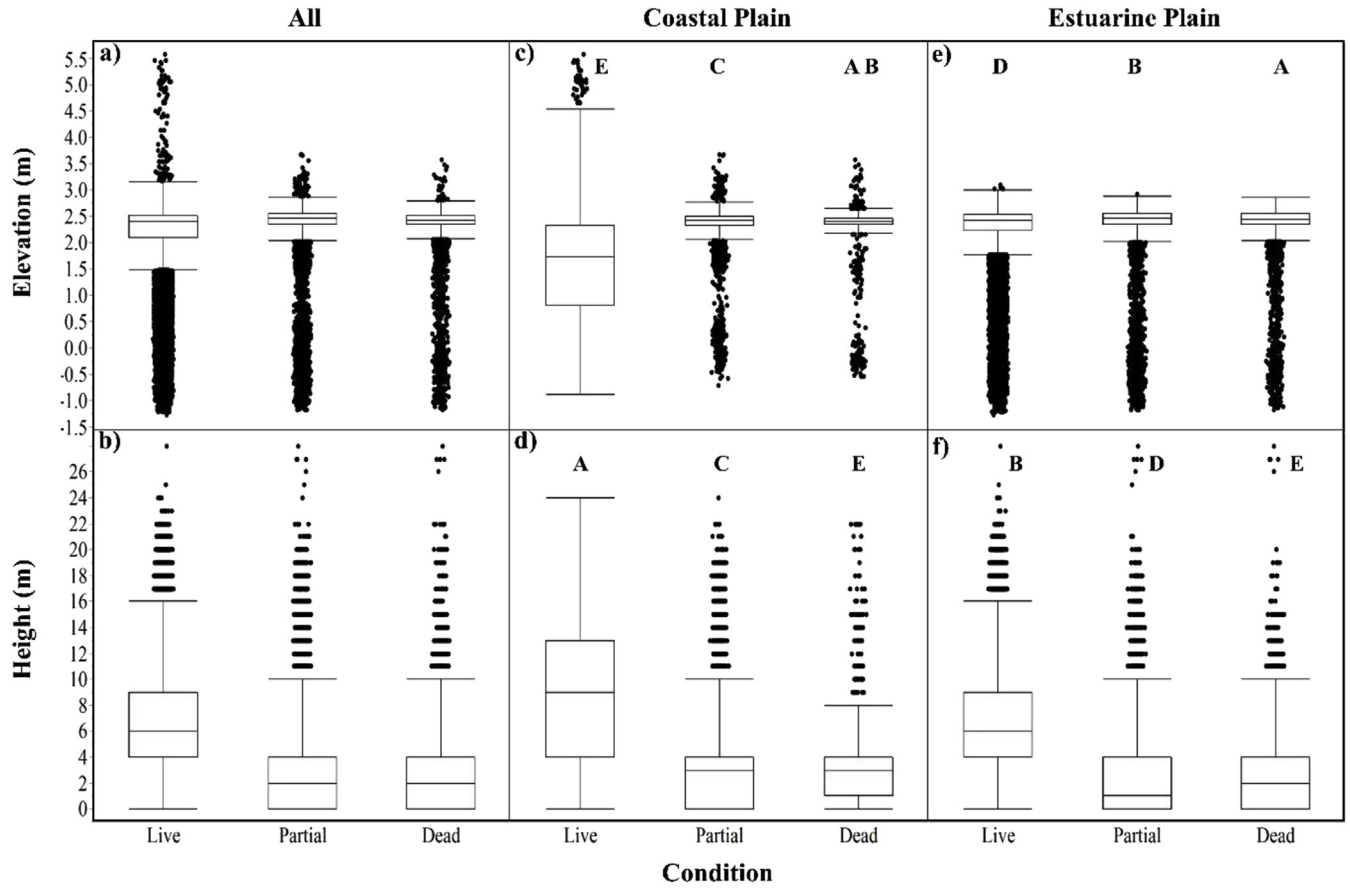

Fig. 7. Box and whiskers plot indicating the variance in elevation of live, partial and dead pixels throughout Kakadu NP (a–b), the coastal plain (c–d) and estuarine plain (e–f). Outcomes not connected by the same letter are significantly different based on post-hoc Tukey HSD.

Macnae, 1966; Saenger and Moverley, 1985). However, time-series observations indicated that *A. marina* trees were largely located in the zone that had exhibited significant landward expansion between 1987 and 2015 and the patterns of colonisation and retreat mirrored changes in mean sea level in the region (Asbridge and Lucas, 2016). Identification of the physiological cause of mangrove dieback was beyond the scope of this remote sensing study, however this study confirms that dieback was related to inundation and sea level.

Our analysis of mangrove heights and vertical distribution of mangrove indicated that our hypotheses were correct: mangroves experiencing dieback were of shorter stature, and typically occurred at higher elevations within the tidal frame, irrespective of their position on the coastal or estuarine plain. The consistency of this pattern and the relationship between the boundary of the impacted mangroves and elevation supports a model of tidal control on both mangrove expansion between 1987 and 2014 and subsequent mangrove dieback in 2015/2016. Whilst strong relationships between ENSO and sea-level fluctuations have been confirmed in Northern Australia (McInnes et al., 2016; White et al., 2014), mean sea-level change correlated best with landward mangrove distribution dynamics and dieback. As the sea level rises, mangroves colonise inland (if the land behind the wetland is free from obstruction) in order to seek more favourable conditions i.e. reduced inundation and inimical sediment dynamics. Moreover, conditions upstream will become more suitable for mangrove proliferation as the upper tidal extent increases and propagules can be dispersed further landward along the creeks and rivers.

4.2. Implications

The Australian landscape is highly adapted to the effects of El Niño events, which may a) influence access to freshwater from precipitation and groundwater reserves, b) modulate mean sea level and tidal regimes, or c) be a combination of both (Gonneea et al., 2013; Meyssignac and Cazenave, 2012; Vera et al., 2012). These events have also been associated with fluctuations in mangrove substrate elevations (Rogers et al., 2006; Rogers and Saintilan, 2009), and changes in mangrove extent at other sites (Lovelock et al., 2017). This study specifically demonstrated that changes in mangrove extent observed in the lower estuarine and coastal reaches of the West Alligator River were significantly related to changes mean sea level, and less so by El Niño intensity in the period coinciding with satellite altimetry data availability (i.e. 1993 onwards). Accordingly, fluctuations in mangrove extent attest to the capacity for mangrove to adapt relatively rapidly to sea-level fluctuations associated with El Niño variability. Mangrove distribution was highly variable with some expansion preferentially occurring along palaeochannels or depressions on the floodplain, whilst other areas exhibited declines or increases in extent as a result of changes in channel migration (Asbridge et al., 2018; pers obs). Despite the scale of the 2015/16 event and limited extent of prior observations of mangrove dieback, palaeoecological evidence indicates that mangrove dieback may not be unprecedented. Changes to ENSO conditions and shifts in Walker Circulation pattern have been reported throughout the Holocene, based on evidence from tropical Northern Australia, with ENSO-scale variability commencing approximately 4000BP (Shulmeister, 1992; Shulmeister and Lees, 1995). Sedimentary records from the late Holocene also indicate sporadic major floods consistent with a reduction in wet season precipitation and large river discharge in northern Australia (Nott and Price, 1999). Aboriginal mollusc exploitation reflects these changes in environmental conditions extending to approximately 500 years ago, thereby demonstrating that

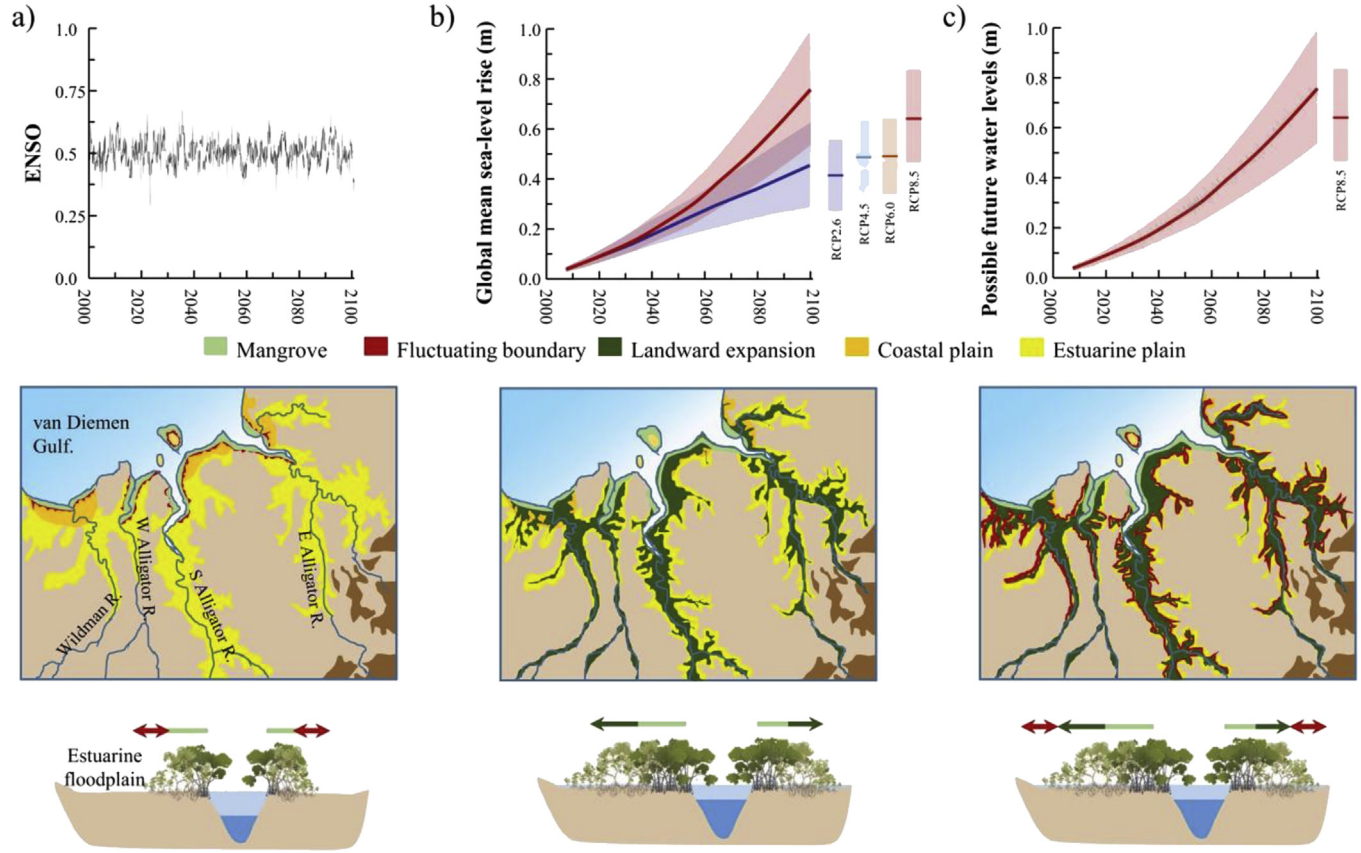

Fig. 8. Conceptual model indicating the effect of a) ENSO-driven sea-level oscillations, b) global sea-level rise, and c) the combined effect of ENSO sea-level oscillations and global sea-level rise on mangrove landward boundaries.

archaeological sites can act as an archive for paleoclimatic indicators (Bourke et al., 2007).

ENSO projections to the end of the 21st century indicate increasing intensity with both El Niño driven drying in the western Pacific Ocean and rainfall increases in the central and eastern equatorial Pacific (Power et al., 2013) and a doubling in the frequency of extreme events (Cai et al., 2014). However, unlike late-Holocene ENSO amplification which coincided with relatively stable conditions, or sea-level falls of 1–2 m (Lewis et al., 2013), the projected 21st century intensification is anticipated to coincide with acceleration in sea-level rise (IPCC et al., 2013). However, stressors associated with sea-level rise and El Niño are not likely to compound, which was recently implied by Harris et al. (2018), as the direction of hydrological change associated with sea-level rise is contrary to that of El Niño-driven sea-level fluctuations. As conceptualised in Fig. 8, we propose that the landward pattern of progressive mangrove expansion and periodic dieback documented in this study is likely to dominate over short timescales coinciding with ENSO variability. However, the overall pattern of change to the end of the 21st century will be landward mangrove extension across estuarine plain in Kakadu NP, which may occur rapidly once a levee is breached or overtopped (Wolanski and Chappell, 1996).

In contrast, it is the La Nina phase of ENSO, which increases sea levels across northern Australia and will compound the effects of sea-level rise in this region, and elsewhere. Given the largely infilled nature of the estuaries of Kakadu NP and expansive estuarine floodplains, substantial lateral space is available for landward expansion throughout the 21st century under these conditions. Of greater concern will be the effects of sea-level rise on saltwater intrusion, which hydrodynamic modelling has indicated will impact substantial areas of freshwater wetlands within Kakadu NP (Bayliss et al., 2018). This will include potential shoreline changes at the open coast, which have already been found to be highly dynamic (Asbridge and Lucas, 2016), and whose geomorphological behaviour with sea-level rise is projected to differ from the more infilled estuarine plains (Woodroffe, 2018).

5. Conclusion

We present evidence from Kakadu NP to support widespread dieback of mangrove throughout northern Australia during 2015/2016 that complements existing evidence from the Gulf of Carpentaria (Duke et al., 2017) and Exmouth (Lovelock et al., 2017). This period coincided with a very strong El Niño event, which by some accounts exceeded the previous strongest recorded event occurring in 1997/98 (See Oceanic Nino Index of NOAA). Identification of the cause of dieback has remained elusive as variations in mean sea level are strongly correlated with ENSO, particularly on the northern and western coastlines of Australia, meaning that the cause of dieback could feasibly be directly related to ENSO through a reduction in sea level, or indirectly as ENSO modulates tidal regimes (McInnes et al., 2016; White et al., 2014). Previous analysis of rainfall, air temperature, regional sea-level anomalies and tide gauge water level fluctuations for mangrove in Kakadu NP failed to differentiate whether the dieback was driven by changes in mean sea level or coincident climatic fluctuation (Lucas et al., 2018). By quantifying the extent and condition of dieback in Kakadu NP, and comparing this to prior changes in mangrove extent, we provide evidence that fluctuations in the landward distribution of mangrove, including dieback, is statistically related to sea-level fluctuation throughout the Arafura and Timor Seas and northern Australia, rather than El Niño intensity, though the two factors can never be entirely differentiated, as demonstrated by Harris et al. (2018). Despite the scale of mangrove dieback observed in Kakadu NP and elsewhere, we propose that the effect of El Niño-related sea-level fluctuations on

mangrove extent will be superimposed on the longer-term trend of sea-level rise, and that the effect of this dieback event and others will be reversed as mangrove continue to expand landward.

Acknowledgements

The authors thank funders who supported this research and associated research of co-authors including the UOW Global Challenges Program, which supported the Blue Carbon futures project, the UOW Faculty of Science, Medicine and Health, the Australian Research Council (FT130100532) and the European Regional Development Fund (ERDF) Ser Cymru Program. The authors also acknowledge the traditional landowners who supported this research, facilitated through Parks Australia (Permit no. RK917d).

Appendix A. Supplementary data

Supplementary data to this article can be found online at https://doi.org/10.1016/j.ecss.2019.106353.

References

Asbridge, E., Lucas, R.M., 2016. Mangrove response to environmental change in Kakadu national park. IEEE J. Sel. Top. Appl. Earth Obs. Remote Sens. 9, 5612–5620.
Asbridge, E., Lucas, R., Accad, A., Dowling, R., 2015. Mangrove response to environmental changes predicted under varying climates: case studies from Australia. Curr. For. Rep. 1, 178–194.
Asbridge, E., Lucas, R., Ticehurst, C., Bunting, P., 2016. Mangrove response to environmental change in Australia's Gulf of Carpentaria. Ecol. Evol. 6, 3523–3539.
Asbridge, E., Lucas, R., Rogers, K., Accad, A., 2018. The extent of mangrove change and potential for recovery following severe Tropical Cyclone Yasi, Hinchinbrook Island, Queensland, Australia. Ecol. Evol. 8, 10416–10434.
Bayliss, P., Saunders, K., Dutra, L.X.C., Melo, L.F.C., Hilton, J., Prakash, M., Woolard, F., 2018. Assessing sea level-rise risks to coastal floodplains in the Kakadu Region, northern Australia, using a tidally driven hydrodynamic model. Mar. Freshw. Res. 69, 1064–1078.
Bourke, P., Brockwell, M.S., Faulkner, P., Meehan, B., 2007. Climate variability in the mid to late Holocene Arnhem Land Region, North Australia: archaeological archives of environmental and cultural change. Archaeol. Ocean. 42, 91–101.
Bunting, P., Rosenqvist, A., Lucas, R., Rebelo, L.M., Hilarides, L., Thomas, N., Hardy, A., Itoh, T., Shimada, M., Finlayson, C., 2018. The global mangrove watch—a new 2010 global baseline of mangrove extent. Remote Sens. 10 (10), 1669.
Cai, W., Borlace, S., Lengaigne, M., van Rensch, P., Collins, M., Vecchi, G., Timmermann, A., Santoso, A., McPhaden, M.J., Wu, L., England, M.H., Wang, G., Guilyardi, E., Jin, F.-F., 2014. Increasing frequency of extreme El Niño events due to greenhouse warming. Nat. Clim. Chang. 4, 111.
Clewley, D., Bunting, P., Shepherd, J., Gillingham, S., Flood, N., Dymond, J., Lucas, R., Armston, J., Moghaddam, M., 2014. A python-based open source system for geographic object-based image analysis (GEOBIA) utilizing raster attribute tables. Remote Sens. 6, 6111–6135.
Dalrymple, R.W., Knight, R.J., Zaitlin, B.A., Middleton, G.V., 1990. Dynamics and facies model of a macrotidal sand-bar complex, cobequid bay—salmon river estuary (Bay of fundy). Sedimentology 37 (4), 577–612.
Danaher, K.F., 1995. Marine Vegetation of Cape York Peninsula. Cape York Peninsula Land Use Strategy. Office of Co-ordinator General of Queensland, Brisbane, Department of the Environment, Sport and Territories, Canberra.
Duke, N.C., Kovacs, J.M., Griffiths, A.D., Preece, L., Hill, D.J.E., van Oosterzee, P., Mackenzie, J., Morning, H.S., Burrows, D., 2017. Large-scale dieback of mangroves in Australia's Gulf of Carpentaria: a severe ecosystem response, coincidental with an unusually extreme weather event. Mar. Freshw. Res. 68, 1816–1829.
Finlayson, C.M., Woodroffe, C.D., 1996. Wetland vegetation of the Alligator Rivers region. In: Finlayson, C.M., von Oertzen, I. (Eds.), Landscape and Vegetation Ecology of the Kakadu Region, Northern Australia. Kluwer, Dordrecht, pp. 81–112.
Finnegan, L.G., 1993. Hydrological characteristics of deep ripping under simulated rainfall at Ranger Uranium Mine. Off. Supervising Sci. 134.
Flores-de-Santiago, F., Kovacs, J.M., Flores-Verdugo, F., 2013. The influence of seasonality in estimating mangrove leaf chlorophyll-a content from hyperspectral data. Wetl. Ecol. Manag. 21, 193–207.
Gonneea, M.E., Mulligan, A.E., Charette, M.A., 2013. Climate-driven sea level anomalies modulate coastal groundwater dynamics and discharge. Geophys. Res. Lett. 40 (11), 2701–2706.
Harris, R.M.B., Beaumont, L.J., Vance, T.R., Tozer, C.R., Remenyi, T.A., Perkins-Kirkpatrick, S.E., Mitchell, P.J., Nicotra, A.B., McGregor, S., Andrew, N.R., Letnic, M., Kearney, M.R., Wernberg, T., Hutley, L.B., Chambers, L.E., Fletcher, M.S., Keatley, M.R., Woodward, C.A., Williamson, G., Duke, N.C., Bowman, D.M.J.S., 2018. Biological responses to the press and pulse of climate trends and extreme events. Nat. Clim. Chang. 8, 579–587.
Hay, T., Gribble, N., De Vries, C., Danaher, K., Dunning, M., Hearnden, M., Caley, P., Wright, C., Brown, I., Bailey, S., 2005. Methods for monitoring the abundance and habitat of the northern Australian mud crab Scylla serrata. Fish. Rep. 80.
Heap, A.D., Bryce, S., Ryan, D.A., 2004. Facies evolution of Holocene estuaries and deltas: a large-sample statistical study from Australia. Sediment. Geol. 168.
IPCC, 2013. In: Stocker, T.F., Qin, D., Plattner, G.-K., Tignor, M., Allen, S.K., Boschung, J., Nauels, A., Xia, Y., Bex, V., Midgley, P.M. (Eds.), Climate Change 2013: the Physical Science Basis. Contribution of Working Group I to the Fifth Assessment Report of the Intergovernmental Panel on Climate Change. Cambridge University Press, Cambridge, United Kingdom and New York, NY, USA, pp. 1535.
Khan, M.A., Aziz, I., 2001. Salinity tolerance in some mangrove species from Pakistan. Wetl. Ecol. Manag. 9, 229–233.
Knighton, A.D., Mills, K., Woodroffe, C.D., 1991. Tidal-creek extension and saltwater intrusion in northern Australia. Geology 19, 831–834.
Lewis, S.E., Sloss, C.R., Murray-Wallace, C.V., Woodroffe, C.D., Smithers, S.G., 2013. Post-glacial sea-level changes around the Australian margin: a review. Quat. Sci. Rev. 74, 115–138.
Lovelock, C.E., Feller, I.C., Reef, R., Hickey, S., Ball, M.C., 2017. Mangrove dieback during fluctuating sea levels. Sci. Rep. 7, 1680.
Lucas, R., Mitchell, A., 2017. Integrated land cover and change classifications. In: Díaz-Delgado, R., Lucas, R., Hurford, C. (Eds.), The Roles of Remote Sensing in Nature Conservation: A Practical Guide and Case Studies. Springer International Publishing, Cham, pp. 295–308.
Lucas, R.M., Milne, A.K., Mitchell, A., Donnelly, B., Ellison, J., 2000. Use of stereo aerial photography for assessing changes in the extent and height of mangrove canopies in tropical Australia, Geoscience and Remote Sensing Symposium. In: 2000. Proceedings. IGARSS 2000. IEEE 2000 International, vol. 1885. pp. 1880–1882.
Lucas, R.M., Ellison, J.C., Mitchell, A., Donnelly, B., Finlayson, M., Milne, A.K., 2002. Use of stereo aerial photography for quantifying changes in the extent and height of mangroves in tropical Australia. Wetl. Ecol. Manag. 10, 159–173.
Lucas, R., Finlayson, C.M., Bartolo, R., Rogers, K., Mitchell, A., Woodroffe, C.D., Asbridge, E., Ens, E., 2018. Historical perspectives on the mangroves of Kakadu national park. Marine and Freshwater Research.
Macnae, W., 1966. Mangroves in eastern and southern Australia. Aust. J. Bot. 14, 67–104.
McInnes, K.L., White, C.J., Haigh, I.D., Hemer, M.A., Hoeke, R.K., Holbrook, N.J., Kiem, A.S., Oliver, E.C.J., Ranasinghe, R., Walsh, K.J.E., Westra, S., Cox, R., 2016. Natural hazards in Australia: sea level and coastal extremes. Clim. Change 139, 69–83.
McQuade, C.V., 1993. Probabilistic Design for Risk Analysis in Mine Water Resources Management Systems. Ph.D. thesis. The University of Queensland, Brisbane.
Merzlyak, M.N., Gitelson, A.A., Chivkunova, O.B., Rakitin, V.Y., 1999. Non-destructive optical detection of pigment changes during leaf senescence and fruit ripening. Physiol. Plant. 106, 135–141.
Meyssignac, B., Cazenave, A., 2012. Sea level: a review of present-day and recent-past changes and variability. J. Geodyn. 58, 96–109.
Mitchell, A.L., Lucas, R.M., Donnelly, B.E., Pfitzner, K., Milne, A.K., Finlayson, M., 2007. A new map of mangroves for Kakadu National Park, Northern Australia, based on stereo aerial photography. Aquat. Conserv. Mar. Freshw. Ecosyst. 17, 446–467.
Muhsoni, F.F., Sambah34, A., Mahmudi, M., Wiadnya, D., 2018. Comparison of different vegetation indices for assessing mangrove denisty using sentinel-2 imagery. Int. J. 14, 42–51.
NOAA/NESDIS/STAR Laboratory for Satellite Altimetry, 2018. Laboratory for Satellite Altimetry/Sea Level Rise: Regional Sea Level Time Series.
Nott, J., Price, D., 1999. Waterfalls, floods and climate change: evidence from tropical Australia. Earth Planet. Sci. Lett. 171, 267–276.
Power, S., Delage, F., Chung, C., Kociuba, G., Keay, K., 2013. Robust twenty-first-century projections of El Niño and related precipitation variability. Nature 502, 541.
Quisthoudt, K., Schmitz, N., Randin, C.F., Dahdouh-Guebas, F., Robert, E.M., Koedam, N., 2012. Temperature variation among mangrove latitudinal range limits worldwide. Trees (Berl.) 26 (6), 1919–1931.
Rogers, K., Saintilan, N., 2009. Predicting the response of coastal wetlands of Southeastern Australia to sea-level rise.
Rogers, K., Wilton, K.M., Saintilan, N., 2006. Vegetation change and surface elevation dynamics in estuarine wetlands of southeast Australia. Estuar. Coast Shelf Sci. 66 (3–4), 559–569.
Saenger, P., Moverley, J., 1985. Vegetative phenology of mangroves along the Queensland coastline. Proc. Ecol. Soc. Aust. 13, 257.
Shulmeister, J., 1992. A Holocene pollen record from lowland tropical Australia. Holocene 2, 107–116.
Shulmeister, J., Lees, B.G., 1995. Pollen evidence from tropical Australia for the onset of an ENSO-dominated climate at c. 4000 BP. Holocene 5, 10–18.
Vera, I., Mariño-Tapia, I., Enriquez, C., 2012. Effects of drought and subtidal sea-level variability on salt intrusion in a coastal karst aquifer. Mar. Freshw. Res. 63 (6), 485–493.
White, N.J., Haigh, I.D., Church, J.A., Koen, T., Watson, C.S., Pritchard, T.R., Watson, P.J., Burgette, R.J., McInnes, K.L., You, Z.-J., Zhang, X., Tregoning, P., 2014. Australian sea levels—trends, regional variability and influencing factors. Earth Sci. Rev. 136, 155–174.
Wolanski, E., Chappell, J., 1996. The response of tropical Australian estuaries to a sea level rise. J. Mar. Syst. 7, 267–279.
Woodroffe, C.D., 1995. Response of tide-dominated mangrove shorelines in Northern Australia to anticipated sea-level rise. Earth Surf. Process. Landforms 20, 65–85.
Woodroffe, C.D., 2018. Mangrove response to sea level rise: palaeoecological insights from macrotidal systems in northern Australia. Mar. Freshw. Res. 69, 917–932.
Woodroffe, C.D., Thom, B.G., Chappell, J., 1985. Development of widespread mangrove swamps in mid-Holocene times in northern Australia. Nature 317, 711–713.
Woodroffe, C.D., Chappell, J., Thom, B.G., Wallensky, E., 1989. Depositional model of a macrotidal estuary and floodplain, South Alligator River, Northern Australia. Sedimentology 36, 737–756.
Woodroffe, C.D., Mulrennan, M.E., Chappell, J., 1993. Estuarine infill and coastal progradation, southern van Diemen Gulf, northern Australia. Sediment. Geol. 83, 257–275.
Woodroffe, C.D., Rogers, K., McKee, K.L., Lovelock, C.E., Mendelssohn, I.A., Saintilan, N., 2016. Mangrove sedimentation and response to relative sea-level rise. Ann. Rev. Mar. Sci. 8, 243–266.